12-2017

Search for the decays of 113Ba

Yongchi Xiao
University of Tennessee, Knoxville, yxiao5@vols.utk.edu

To the Graduate Council:

I am submitting herewith a dissertation written by Yongchi Xiao entitled "Search for the decays of 113Ba." I have examined the final electronic copy of this dissertation for form and content and recommend that it be accepted in partial fulfillment of the requirements for the degree of Doctor of Philosophy, with a major in Physics.

Robert Grzywacz, Major Professor

We have read this dissertation and recommend its acceptance:

Soren Sorensen, Thomas Papenbrock, Guillermo Ivan Maldonado

Accepted for the Council:

Dixie L. Thompson

Vice Provost and Dean of the Graduate School

(Original signatures are on file with official student records.)

Search for the decays of 113Ba

A Dissertation Presented for the

Doctor of Philosophy

Degree

The University of Tennessee, Knoxville

Yongchi Xiao

December 2017

In memory of my beloved grandfather Yongyu Liu.

Acknowledgements

First of all, I would like to express my deepest thanks to my advisor Dr. Robert Grzywacz for his comprehensive and thorough academic guidance, great patience and kind personality. He is the best advisor a student can expect. He is the man I will learn from forever.

I would like to thank Dr. Karolina Kolos, Dr. Shintaro Go and Dr. Stanley Paulauskas who brought me to the very details of experimental nuclear physics at the beginning of my graduate research. What I learnt from them includes not only data analysis, device testing and programming, but also scientific thinking which is the key for a graduate student. They are the teachers as well as my friends. I will never forget the busy yet happy days we spent together.

My gratitude goes to Dr. Krzysztof Rykaczewski, Dr. Carl Gross, Dr. Chiara Mazzocchi, Dr. Katsuhisa Nishio and Dr. Riccardo Orlandi, with whom I participated in experiments in Japan Atomic Energy Agency. Thank you for providing me the opportunities to join a group of real scientists in world-class research. My research would not have been able to move forward without your help. I also want to thank my committee members, Dr. Soren Sorensen, Dr. Thomas Papenbrock and Dr. Guillermo Ivan Maldonado for your insightful comments and constructive criticism which drives me dive deeper into my research for the answer.

I would like to say thank you to my colleagues and friends, especially Dr. Marija Vostinar, Dr. Callie Goetz, Mr Steven Taylor and Mr Toby King. Thank you for your selfless help during these years no matter in academic areas or daily life. It is my great pleasure to meet and work with you all here.

Finally, I must thank my wife Dr. Xinyi Lu with whom I shared my entire graduate life, built up my home together and stay energetic and optimistic. I must thank my parents, Fuyin Xiao and Keli Liu, for your love in bringing me up and encouraging me to pursue my new life on the other side of the Pacific Ocean. I must thank my mother in-law, Yue Wang, for bringing me a good wife, as well as all my family members for your understanding my life in the US, which is far more than I can put on paper.

Better go back and make a net than long for the fish by merely staring into the water.

Dong Zhongshu

Abstract

The search for new alpha-emitters in the region above tin-100 was carried out in Japan Atomic Energy Agency (JAEA) tandem accelerator in Tokai, Japan. This work aimed to discover barium-113 produced via the fusion-evaporation reaction nickel-58(nickel-58,3n)barium-113 and observation through its alpha-decay chain from barium-113 to xenon-109 to tellurium-105 and tin-101. In the proof of principle experiment in March 2014, the alpha-decay chain of xenon-109 was observed with Double-sided Silicon Strip Detector (DSSD) and digital electronics at JAEA Recoil Mass Separator (RMS). The first discovery-oriented barium-113 experiment was carried out in December 2014 searching for its alpha-decay, ground-state to ground-state beta-decay and beta-delayed charged particle emission. An estimate was made on the upper limit of half-life of barium-113 as well as the production cross section.

Table of Contents

List of Tables

List of Figures

Chapter 1

Introduction

The search for the "super-allowed" α-decay above the doubly-magic nucleus ^{100}Sn is conducted through a series of experiments. Two experiments performed in this region are described in this thesis. The first experiment measured ^{109}Xe decay and aimed to prove the technical capabilities of our experimental system and the second is aimed at the discovery of ^{113}Ba. The motivation also includes the need for understanding the limits of stability near the $N = Z$ line. Direct measurement of ^{113}Ba decay modes provides essential physical properties such as decay energy Q_α, half-life $T_{1/2}$. It is also very important to provide a quantitative determination of different competing decay modes.

In Chapter 2, the theoretical background including influence of shell model on α-decay mechanism and the relevant previous work in ^{100}Sn region are reviewed. The motivation for experiment searching for ^{113}Ba is explained in detail. Chapter 3 describes the experimental setup. In Chapter 4, detailed analysis of data is given. In Chapter 5, discussion with theoretical calculation is presented. The summary is given in Chapter 6.

Chapter 2

Backgrounds and Motivation

2.1 An Overview of α-decay

α-decay is a spontaneous process where an α-particle is emitted from a mother nucleus. The α-decay energy Q_α is given as:

$$Q_\alpha({}^{A}_{Z}X_N) = (BE(A-4, Z-2) + 28.3MeV) - BE(A, Z) \tag{2.1}$$

where 28.3 MeV is the binding energy of an α-particle. When this quantity becomes negative, the α-particle will no longer be bound and the decay can occur spontaneously. From the semi-empirical Bethe-Weizsacker formula for binding energy based on liquid drop model, the difference in the binding energy of mother and daughter nucleus can be written as the function of Z and A [1]:

$$Q_\alpha = 48.88\frac{1}{A^{1/3}} - 92.80(1 - \frac{2Z}{A})^2 + 2.856\frac{Z}{A^{1/3}}(1 - \frac{Z}{3A}) - 35.04 \tag{2.2}$$

and provides us with a phenomenological estimate how the decay energy Q_α changes with increasing N number within a given isotopic chain. This equation suggests that the first few positive values for Q_α appear around A=142 and provides a explanation for the fact that α-decay usually occurs for $A \geq$140 region.

The known half-lives of α-decay span in a wide range where the longest(^{144}Nd) is 5×10^{29} times as long as that of ^{212}Po. Approximately, the relation between α-decay energy and the half-life can be described by the Geiger-Nuttall law [2]:

$$log(T_{1/2}) = AQ_{\alpha}^{-1/2} + B \tag{2.3}$$

where the coefficients A and B can be determined from the experimental values.

In the classical Gamow picture of α-decay [3], it is assumed that an α-particle is existed inside a nucleus and moving independently. At the border of the nucleus, it will be confined by the potential:

$$U(r) = U_{Coulomb} + U_{Centrifugal} \tag{2.4}$$

where:

$$U_{Coulomb} = \frac{2Z_D e^2}{4\pi\epsilon_0 \cdot r}, U_{Centrifugal} = \frac{l(l+1)\hbar^2}{2M_\alpha r^2} \tag{2.5}$$

By applying the WKB-approximation method for tunnelling through the potential barrier, the penetration probability of an α-particle is:

$$P_\alpha \propto exp(-2\int_{R_i}^{R_f} \sqrt{\frac{2M_\alpha(U(r) - Q_\alpha)}{\hbar^2}} dr) \tag{2.6}$$

where M_α is the reduced mass of the α-particle and the daughter nucleus. Since the decay constant λ_α is the probability of the occurrence of α-decay in a unit time, we have:

$$\lambda_\alpha = fP_\alpha \tag{2.7}$$

where f is the frequency of an α-particle colliding with the potential barrier.

On one hand, however, due to the Pauli's blocking effects, it is impossible for an α-particle to be formed deep inside the mother nucleus. On the other hand, the Formula 2.7 describes the α-decays between ground-state to ground-state of even-even nuclei. In many other cases, especially for odd-odd nuclei, discrepancy emerges between theoretical predictions and experimental values for half-lives. It can be explained by the fact that the

α-particle is in fact formed during the decay process instead of being existed long before it and this introduces additional dependence of α-decay on nuclear structure.

2.2 Nuclear Shell Structure

One of the signatures of the emergence of the nuclear shell structure in the atomic nuclear is the discontinuity of nucleon separation energies S_p and S_n at certain numbers such as 2, 8, 20, 28, 50 and 82. Phenomenologically, the nuclear structure can be reproduced by using a central potential (e.g. the harmonic oscillator) plus the spin-orbital interaction term [4]:

$$U(r) = -U_0 + \frac{1}{2}m\omega^2 r^2 - \frac{2}{\hbar^2}\alpha \hat{l} \cdot \hat{s} \tag{2.8}$$

Good agreement with the experimental data can be obtained with the more realistic Woods-Saxon potential [5]:

$$U(r) = \frac{U_0}{1 + exp((r - R_0)/a)} + \frac{U_{ls}}{{r_0}^2}\frac{1}{r}\frac{d}{dr}(\frac{1}{exp((r - R_0)/a)})\hat{l} \cdot \hat{s} \tag{2.9}$$

where

$$U_0 = (-51 + 33(N - Z)/A)MeV \tag{2.10}$$

$$U_{ls} = -0.44U_0 \tag{2.11}$$

The choice of parameters of the W-S potential connects this phenomenological model to the physical properties of the nucleus such as radius and number of nucleons. More modern models are able to explain the emergence of the magic numbers self-consistently and link them to nucleon-nucleon interaction.

The nuclear shell structure is also reflected in the systematics of α-decay energies (Q_α) in α-decay within the same isotopic chain. Typically, the Q_α decreases with increasing neutron numbers. But for example in the case of Bi, Po, At and Rn with A from 209 to 213, the slope abruptly becomes positive (see Figure 2.1 [6]) which here coincides with N=126 magic number. The nuclei $^{211}_{83}$Bi, $^{212}_{84}$Po and $^{213}_{85}$At come with two more neutrons than the neutron

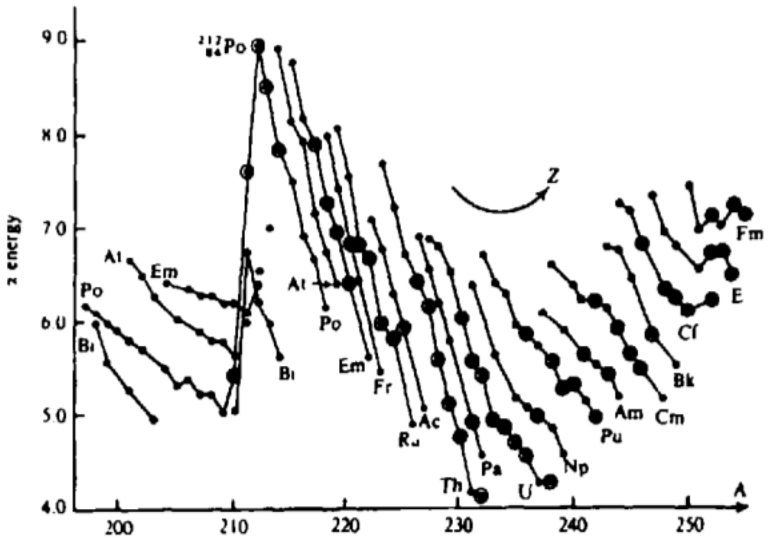

Figure 2.1: The α-decay energy in the mass region $200 \leq A \leq 260$. Different isotopic chains are connected by lines. The large and rapid variation around A=212 indicates evidence for nuclear shell structure due to the presence of shell closure in ^{208}Pb.

magic number N=126 and thus become more unstable against the α-decay. In contrast, the nuclei $^{209}_{83}$Bi, $^{210}_{84}$Po and $^{211}_{85}$At are magic nuclei with N=126 whose α-decay daughter are less stable with two less neutrons. Therefore, the decay energy Q_α is relatively smaller for them.

In the nuclear shell model, nucleons are filled successively into single particle levels separated by shell gaps (see Figure 2.2). In addition to the mean field, nucleons on the same levels with opposite magnetic quantum numbers correlate with each other through the pairing interaction. It is the most crucial correlation beyond the nuclear mean field and leads to zero angular momentum for the ground-states of all observed even-even nuclei, which is responsible for the two-nucleon correlation. Therefore, the clusterization of four nucleons could be a result of such correlation and may finally lead to the preformation of an α-particle. Thus, the α-decay probability is re-written as:

$$\lambda_\alpha = S^\alpha f P_\alpha \tag{2.12}$$

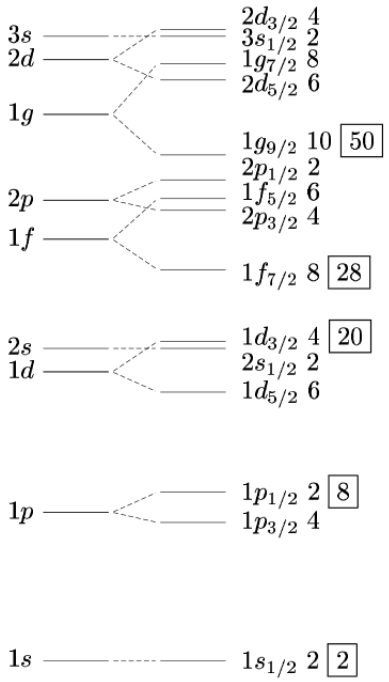

Figure 2.2: Single particle spectrum with partial and accumulated nucleon numbers

where S^{α} is the preformation probability. The pairing correlation strongly enhances the calculated α-decay width and governs the preformation of an α-particle near the nuclear surface [7]. By introducing the reduced decay width [8]:

$$\delta^2 = \frac{h\lambda_{\alpha}}{P_{\alpha}} \tag{2.13}$$

which is the overlap of wavefunctions of the daughter nucleus $\psi_i(A-4)$ times the α-particle wavefunction ϕ_{α} and the mother nucleus wavefunction $\psi_i(A)$:

$$\delta^2 = |\langle \phi_i(A) | \phi_f(A-4) \cdot \phi_{\alpha}(4) \rangle|^2 \tag{2.14}$$

the dependence on penetrability P_{α} is removed. The preformation of an α-particle can be quantified by comparing the reduced decay width [9] to that of ^{212}Po:

$$W_{\alpha} = \frac{\delta^2}{\delta^2(^{212}Po)} \tag{2.15}$$

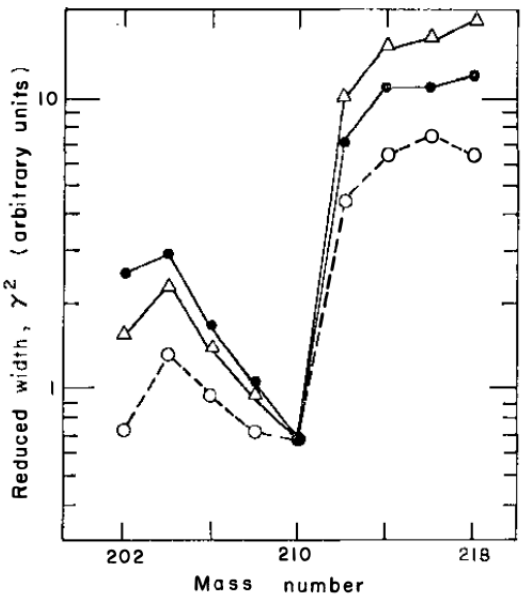

Figure 2.3: Reduced decay width of even-even Po isotopes around $A = 210$ in arbitrary units. The solid circle represent values computed from measured decay constants with the help of Igo's optical potential. The triangles represent values computed from measured decay constants with a pure Coulomb potential used with a cut-off. The open circles represent results calculated from shell model.

As seen above, the α-decay ^{212}Po $\rightarrow$ ^{208}Pb is usually taken as an example and a reference. ^{212}Po has two neutrons and two protons beyond the doubly magic nucleus ^{208}Pb with N=126 and Z=82. A fully microscopic calculation employing four-nucleon wave functions derived from shell model was performed in Reference [10] to determine the pre-formation probability of an α-particle inside even-even Po isotopes. Even though the absolute value was not calculated, the relative reduced decay width normalized to that of ^{210}Po was obtained. As shown in Figure 2.3 [10], there is a sudden jump in the reduced decay width beyond $A = 210$ which is related to the magic number $N = 126$. This is a strong indication of the influence of nuclear shell structure on the pre-formation of an α-particle. The latest microscopic calculation employing the quartetting wave function again confirmed that for even-even Po isotopes, the α-particle formation probabilities experiences a sudden increase beyond $A = 210$. [11]

Within the shell model framework, the wave function for the α-decay ^{212}Po $\rightarrow$ ^{208}Pb can be described as [12]:

$$|^{212}Po(\alpha_4)\rangle = \Sigma_{\alpha_2\beta_2} X(\alpha_2\beta_2;\alpha_4)|^{210}Pb(\alpha_2) \otimes^{210} Po(\beta_2)\rangle \tag{2.16}$$

where α_2, β_2 represents two-neutron and two-proton pairing states. If the neutron-proton interaction is negligible [13], only one configuration will be involved where paired neutrons/protons with total zero angular momentum couple with each other. This can be described and calculated as a collective vibrational states, i.e. $|^{212}\text{Po(gs)}\rangle = |^{210}\text{Pb(gs)}\otimes^{210}\text{Po(gs)}\rangle$. This theoretical approximation is reasonable because of the fact that valence neutrons lying in the much lower state $1h_{9/2}$ are very different from valence protons in $2g_{9/2}$ state. Therefore, the neutron-proton interaction is weak. However, for α-decays of $N \approx Z$ nuclei, such interaction is expected to be enhanced since neutrons and protons are now lying in closely spaced single particle orbitals.

2.3 α-decay Island Above ^{100}Sn Region

Nuclei far away from the β stability valley of the nuclear landscape exhibit a variety of decay properties. They become unstable against nucleon emission as protons and drip lines are approached. The presence of the α-decay island above ^{100}Sn (see Figure 2.4 [14]) is a strong indication of the $N = Z = 50$ shell-closure since the first observation of α-decay in this region in 1960s [15]. Valence neutrons and protons are expected to occupy the same single particle orbitals $d_{5/2}$ and $g_{7/2}$ outside the shell-closure. It has been hypothesized that the α-particle preformation probability might be increased a result of enhanced isovector spin aligned nn, np, pp configuration with $T = 1$ and isoscalar spin anti-aligned np configuration with $T = 0$. If this is confirmed experimentally, it will be revealed by systematically shorter life-time against α-decay, which could finally lead to the enhanced (super-allowed) α-decay [15, 16] with large reduced decay width. The best example of this decay should be ^{104}Te $\rightarrow$ ^{100}Sn where ^{104}Te can be pictured as ^{100}Sn+ α-particle molecule.

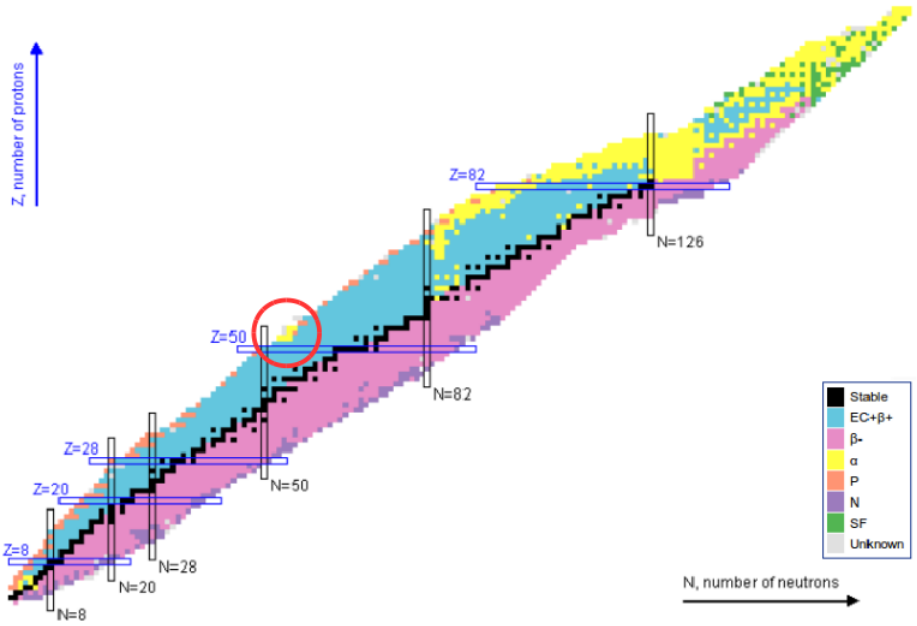

Figure 2.4: Island of alpha-decay above ^{100}Sn (N=Z=50) region shown in the red circle.

Up to now, the latest theoretical calculation has employed np interaction within the framework of a generalized BCS approach in a deformed Woods-Saxon potential [17]. Paired protons and neutrons with the same projected angular momentum are taken into account as the modest enhancement of clustering. From the calculation operated for ^{102}Te and ^{102}Sn, it is pointed out that significant enhancement of four-body clustering is present [18] which sheds light on the greater preformation probability of an α-particle. Meanwhile, a microscopic calculation starting from shell model wave functions [19] which is successful in reproducing the α-decay of ^{212}Po predicts that there is not such "super-allowed" α-decay of ^{104}Te since the pre-formation of an α-particle is calculated to be small and the partial half-life of it is predicted to be very long. Only $T = 1$ isospin configuration was considered in this calculation, which is good for α-decay of ^{212}Po. The discrepancy between different theoretical calculations drives the experimental efforts to clarify this point: whether or not the proton-neutron interaction interaction plays an unique and important role in the enhancement of pre-formation of α-particles in ^{100}Sn region. Correspondingly, the relative simple nucleon

Table 2.1: Table of experimentally measured alpha-decaying Te, I, Xe and Cs isotopes above ^{100}Sn and their half-life $T_{1/2}$, alpha-decay branching ratio b_α and α-decay energies Q_α.

Nucleus	$T_{1/2}$(s)	b_α(%)	E_α(keV)	Reference
^{105}Te	$(620\pm70)\times10^{-9}$	∼100	5069±3	[20]
^{106}Te	$(70^{+20}_{-10})\times10^{-6}$	∼100	4290±9	[22]
^{107}Te	$(3.1\pm0.1)\times10^{-3}$	70±30	4008±5	[23, 24, 25]
^{108}Te	2.1±0.1	49±4	3420±8	[23, 24, 25, 26]
^{109}Te	4.6±0.3	3.9±1.3	3198±6	[23, 24, 26, 27]
^{110}Te	18.6±0.8	∼0.003	2699±8	[26, 28]
^{108}I	$(36\pm6)\times10^{-9}$	91±15	4100±5	[25]
^{109}I	$(103\pm5)\times10^{-9}$	$(1.4\pm0.4)\times10^{-4}$	3918±21	[29]
^{110}I	0.65±0.2	17±4	3580±5	[23, 25, 26]
^{111}I	2.5±0.2	∼0.088	3275±5	[30, 31]
^{112}I	3.42±0.11	∼0.0012	2957±12	[30]
^{113}I	6.6±0.2	3.3×10^{-7}	2707±10	[26, 27]
^{109}Xe	$(13\pm2)\times10^{-3}$	∼100	4217±7	[20]
^{110}Xe	∼0.15	64∼35	3875±11	[23, 26]
^{111}Xe	0.74±0.20	8±8	3720±5	[23, 25]
^{112}Xe	2.7±0.8	0.9±0.8	3330±6	[25, 26]
^{113}Xe	2.74±0.08	∼0.011	3087±8	[25, 27]
^{114}Cs	0.57±0.02	0.018±0.006	3360±5	[28, 30]
^{114}Ba	0.38^{+190}_{-110}	0.9±0.3	3530±4	[22, 32]

configuration outside doubly shell closure ^{100}Sn provides us a perfect playground to test the np interaction.

A number of α-emitters including isotopes of neutron-deficient tellurium, isodine, xenon and caesium have been studied with measurement of half-life, branching ratio and α-decay energy (see Table 2.1). Currently, the ^{105}Te nucleus is the already known lightest α-emitter in this region whose half-life is as short as 0.62 μs which exhibits some properties of the super-allowed α-decay [20, 21].

2.4 Motivation for ^{113}Ba

As mentioned above, the ultimate super-allowed α-decay ^{104}Te → ^{100}Sn has not been discovered yet. Considering the expected value for the half-life of ^{104}Te as short as 40 ns

[33], it will be difficult to transmit the directly produced ^{104}Te nucleus through the electromagnetic separation devices. Therefore, one has to rely on the indirect production of it starting from α-decay predecessor ^{108}Xe or ^{112}Ba whose life-time is on the order of a fraction of a second [33]. While the nearest α-decay chain $^{109}\mathrm{Xe} \rightarrow {}^{105}\mathrm{Te} \rightarrow {}^{101}\mathrm{Sn}$ has been discovered in HRIBF, Oak Ridge National Lab [20], the full chain from ^{113}Ba remains to be measured. Several attempts [32, 34] have been made since 2000s aimed at discovery of ^{113}Ba without firm evidence for the existence of this very exotic isotope. Thus, before producing ^{104}Te via α-decay chain starting from ^{112}Ba, it is necessary to make measurement on the less exotic barium isotope ^{113}Ba with one less neutron than the already-known lightest α-decaying barium isotope ^{114}Ba.

Neutron-deficient barium isotopes are located on the northern border of the island of α-emitters above ^{100}Sn. ^{114}Ba was first observed through its β-decay [35] and later through its α-decay branch [32]. The branching ratio was measured to be b_α=0.93% with decay energy Q_α=3.540 MeV. The total half-life of this isotope was measured to be 0.43 second (the latest measurement gives $T_{1/2}$=380^{+190}_{-110} ms [22]). Even though the absolute branching ratio for α-decay of ^{114}Ba is very small, the relative reduced width of it compared to that of ^{212}Po, $W_\alpha = 16^{12}_{-7}$ is large and could be indicative of strong α-preformation probability (the recent value was adjusted to 6^{+4}_{-3} [22]). The measurement of its more neutron-deficient neighbour ^{113}Ba may help establish the systematics of α-preformation and decay energies for barium isotopes, particularly in context of the recent theoretical work [19]. Because the binding energy landscape is relatively smooth in this region far away from ^{100}Sn, the dominant decay mode of ^{113}Ba is expected to be β^+/EC as that of ^{114}Ba. These barium isotopes were also considered as candidates for heavy cluster emission (^{12}C) with $Q_{^{12}C}$=19.00 MeV with extremely small branching ratio $b_{^{12}C} = 3 \times 10^{-3}$% [36].

The motivation for searching for the decay of the new isotope ^{113}Ba is needed to establish the systematics of binding energies near border line of nuclear existence and the role of the proximity of the $N = Z$ line. There are several particle decay channels potentially occurring in the disintegration of ^{113}Ba. Establishing the dominant decay mode of the $Z = N+1$ ^{113}Ba

is helpful in predicting the border line of $N \sim Z$ nuclear bound systems and answering the question which is the heaviest $N = Z$ bound nucleus experimentally.

One of the main difficulties in studying very exotic nuclei far away from the stability valley is the rapidly decreasing production rate [37]. By recording the the total dose of the ion beam and comparing it with the number of decay events of ^{113}Ba, it is possible to deduce the experimental reaction cross section for this isotope as well as the systematics of exotic barium isotopes. It may help with correcting the theoretical prediction given by statistical model for fusion-evaporation reactions.

2.5 Search for ^{113}Ba

The experiment described in this dissertation is focused on search for the α-decay branch of ^{113}Ba. The experimental designs were based on predictions for decay energies and the amount of α clusterization in this region. The partial half-life $T_{1/2,\alpha}$ of ^{113}Ba is predicted to be around 0.54 s or 0.76 s depending on different models [33]. Based on the extrapolation from less exotic barium isotopes, the Q_{EC} is evaluated to be around 12 MeV. This results in the partial half-life for β-decay about 100 ms [38], which leads to the total half-life between 55-62 ms and the α-decay branching ratio between 11 % and 16 %. A possible two step mode of the possible β-decay, β-delayed proton/α-particle emission can also occur. Therefore, these three decay paths were considered. The search for ^{113}Ba and its subsequent α-decay chain down to ^{101}Sn is most favoured since it will provide a highly selective signal and should allow the identification of this isotope by recording the piled up α-decay pulse traces even if only very few of such chains were observed. The β-decay daughter of ^{113}Ba, ^{113}Cs, with proton decay branching ratio up to 100 %, can be used to search for the ground-state to ground-state β-decay of ^{113}Ba. The β-delayed α-particle emission path $^{113}\text{Ba} \rightarrow {}^{113}\text{Cs} \rightarrow {}^{109}\text{I} \rightarrow {}^{108}\text{Te}$ was also considered.

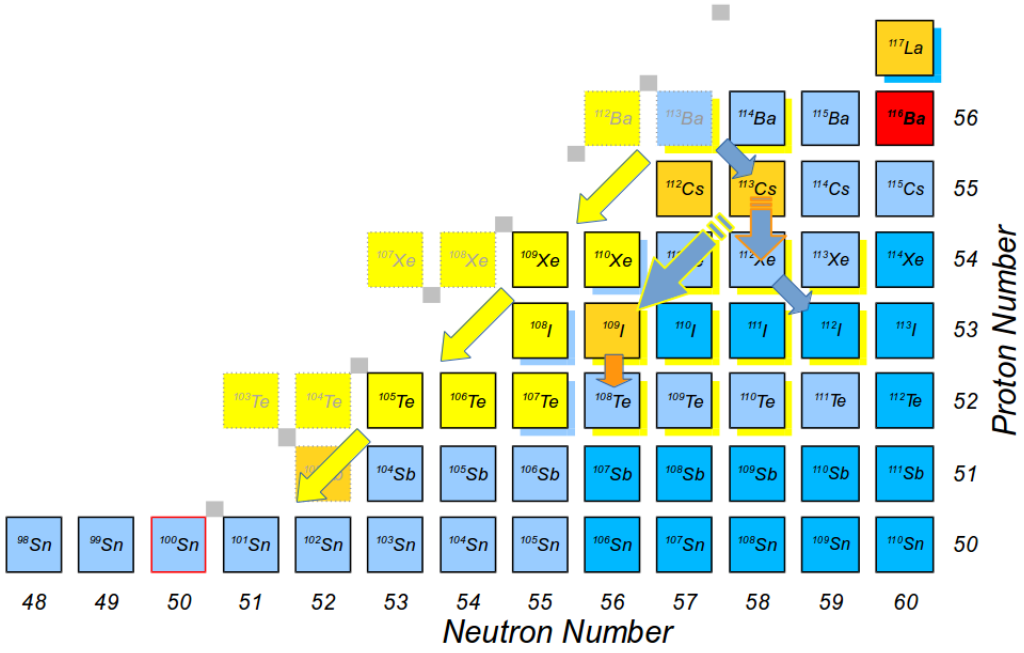

Figure 2.5: Three potential decay paths of ^{113}Ba.

Chapter 3

Experimental Setup

3.1 The JAEA Tandem Accelerator Facility

This experiment, along with the previous proof-of-principle experiment was performed in tandem acceleration facility [39] in Japan Atomic Energy Agency (JAEA), Tokai, Japan. A schematic view of this facility is shown below in Figure 3.1. Negative ions are produced in the source and accelerated to top of the tandem accelerator. Upon arriving at the high voltage terminal, ions go through an electron stripper (carbon foil) and become positively charged. The highly charged positive ions are accelerated down to the exit. The JAEA tandem accelerator is able to accelerate as many as 200 nuclides of 50 elements with the energy accuracy of 100 keV and the operation voltage up to 18 MV.

3.2 Beam and Target

In the ^{113}Ba experiment, a ^{58}Ni beam at the energy of 245 and 250 MeV respectively bombard the target made of ^{58}Ni with the average intensity of 36.6 pn·A. The ^{113}Ba ions were expected to be produced via the fusion-evaporation reaction ^{58}Ni(^{58}Ni,3n)^{113}Ba. The target at the thickness of 520 μg/cm^2 was mounted onto a target holder which was rotating at the frequency of 6 Hz. It is segmented into 4 equal sectors (see Figure 3.2) with a gap between

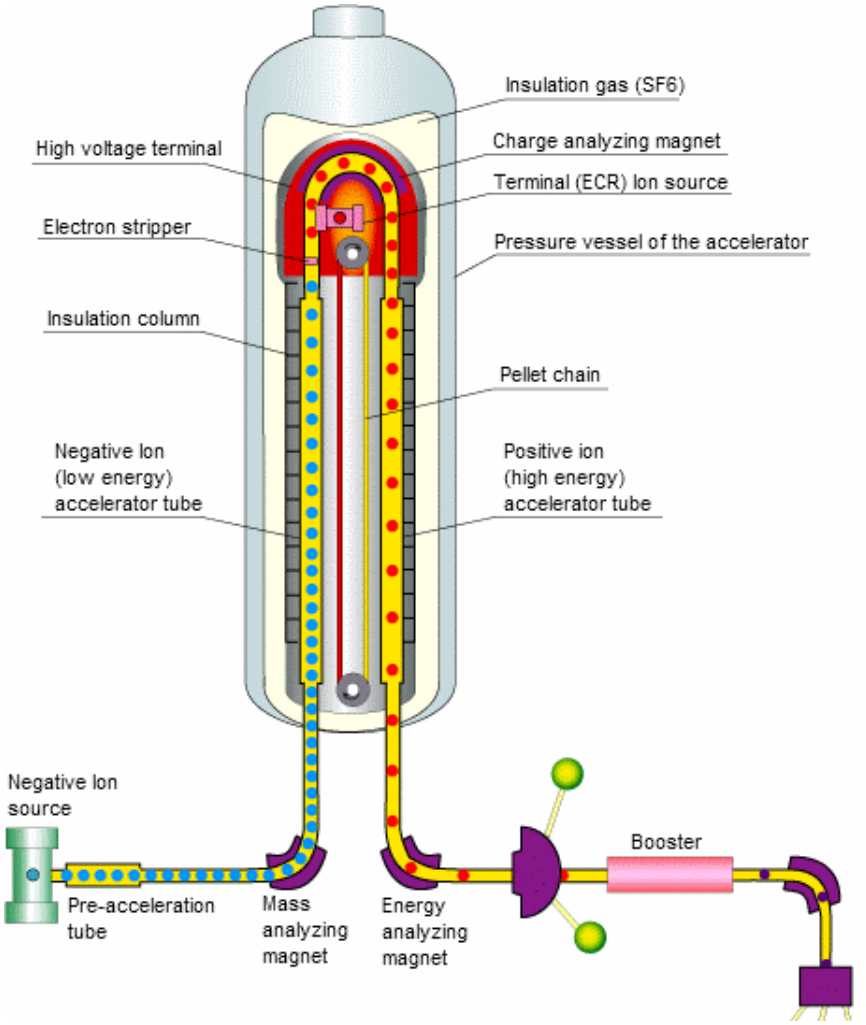

Figure 3.1: A schematic drawing of the tandem accelerator at JAEA.

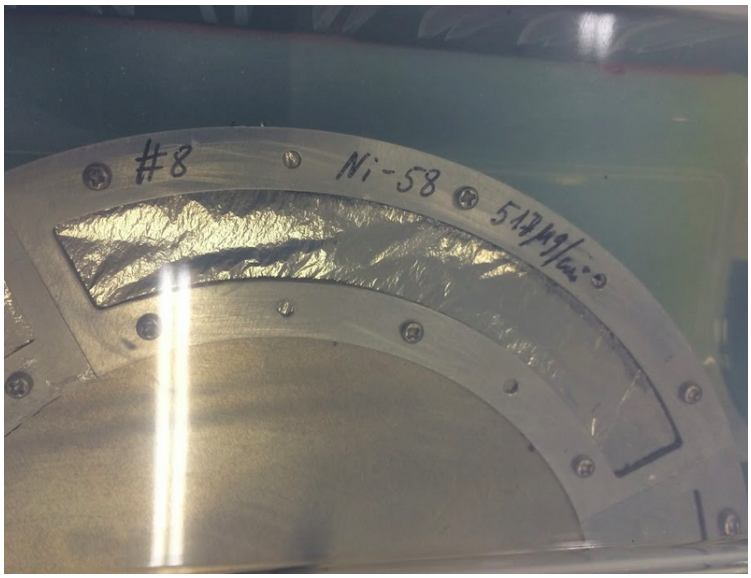

Figure 3.2: The sector of thin foil made of ^{58}Ni is the target.

adjacent sectors. The beam will be automatically blocked to avoid effects of scattering off the edge of the target frame. The target foils were manufactured at GSI target laboratory.

3.3 Recoil Mass Separator

Following the fusion-evaporation reaction, the recoil products were sent to the Recoil Mass Separator (RMS) [40] which plays a key role in separation of various reaction products. The schematic layout is shown in Figure 3.3. The RMS has a symmetric configuration of Q_1Q_2-ED_1-MD-ED_2-Q_3Q_4-O. Two 25° electric dipoles (ED_1 and ED_2) and one -50° magnetic dipole (MD) disperse reaction products by their mass/charge (A/Q) ratio and cancel out the energy/charge dispersion. Two quadrupole doublets (Q_1Q_2 and Q_3Q_4) allow to focus the recoils irrespective of their angular spread and also to change the A/Q dispersion at the focal planes. The octupole magnet (O) is for the correction of a non-linearity of the A/Q dispersion. These electric and magnetic components are arranged on a rotating platform (-5° to 40°), 9.4m in length.

The RMS is designed to reduce a background originating from the scattered beams from the anode surface of the ED_1. For this purpose, the ED_1 anode is vertically split into two

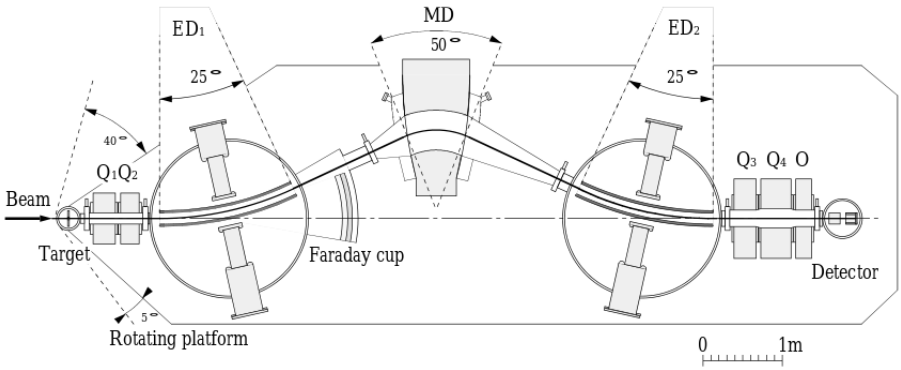

Figure 3.3: A schematic view of the Recoil Mass Separator (RMS) at JAEA.

parts separated by 1cm so that the primary beam can pass through this gap without hitting the anode surface.

The mass resolution of the RMS is $A/\Delta A \simeq 300$. The solid angles were 11 and 21 msr for the focusing condition with mass dispersion of 1.1 and 0cm/%. A transmission efficiency is assumed to be 5% in this experiment.

In this experiment for ^{113}Ba, the RMS was set with A=113, Q=27. The energy of accepted recoils at the focal plane of the RMS was set to 106 MeV.

3.4 Detectors at RMS Focal Plane

An implantation chamber is placed right behind the focal plane of the RMS. In front of it is the multi-wire proportional chamber (MWPC). A double-sided silicon detector (DSSD) as well as two Si-PIN detector are placed inside the chamber. The whole chamber is in the concave formed by a large array of γ-ray NaI detectors. The schematic drawing of the whole set-up is shown in the Figure 3.4 below.

3.4.1 Multi-wire Proportional Chamber

Right in front of the focal plane of the RMS, a slit was placed and adjusted to let only a component beam with optimum A/Q ratio=113/127 enter the implantation chamber (see Figure 3.6). A multi-wire proportional chamber was placed behind the slit, in front of the

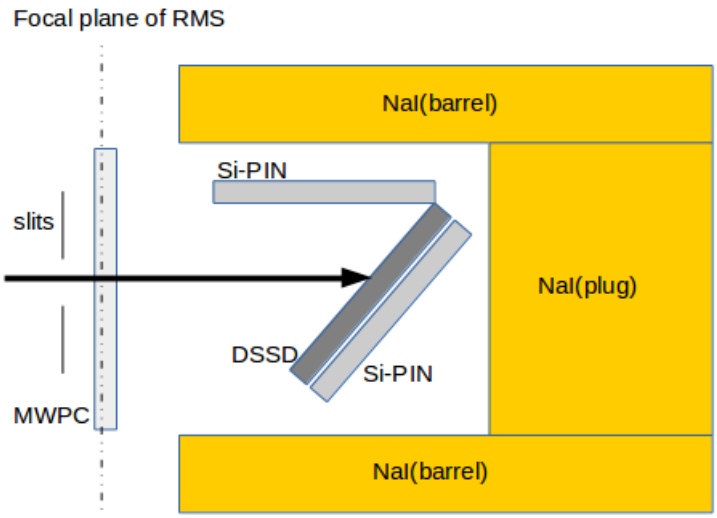

Figure 3.4: A schematic drawing of the configuration of all detectors near the focal plane of the RMS viewed from top. The black arrow indicates the direction in which the recoil ions propagate.

DSSD. It is used for obtaining the energy loss of ions passing through versus the horizontal distribution of them so that precise determination of different components of ions can be made. Incoming beam has to pass through the MWPC before they get to DSSD. Thus, signals from MWPC can be utilized to veto ion implantations on DSSD.

3.4.2 Double-sided Silicon Detector

The double-sided silicon strip detector (DSSD) is the core detector in this experiment. It is 4 cm by 4 cm, 65 μm thick and segmented into 40 strips horizontally on the front and vertically on the back. It is used to detect residues from fusion-evaporation reaction and their decay products. The typical energy of recoiling residues falls between 37 MeV and 48 MeV due to the loss of a fraction of 106 MeV kinetic energy after passing MWPC. The energy of protons, α-particles and β-delayed charged particles ranges from 800 keV up to several MeV. The DSSD is inclined by 45 degrees with respect to the incoming beam. Therefore, the radiation damage of the DSSD is reduced during the period of 10-days experiment with

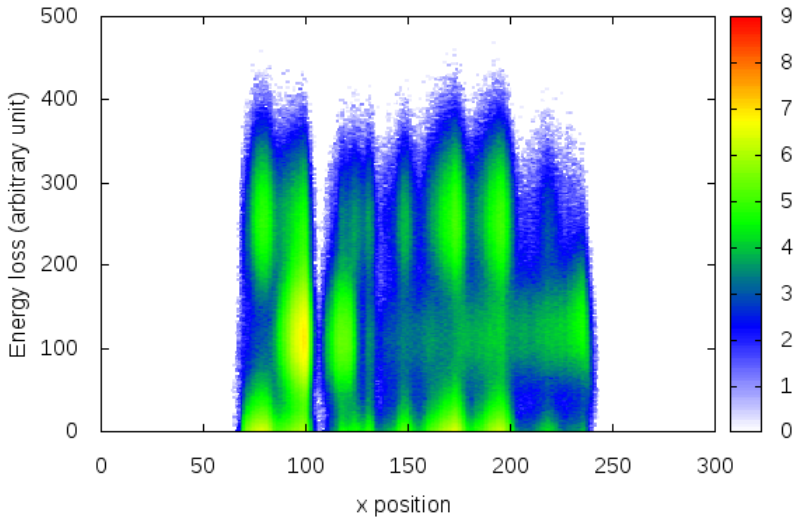

Figure 3.5: Energy loss of ions passing through the MWPC versus horizontal position of ions with slits wide open letting in all components during the test run in the proof-of-principle experiment.

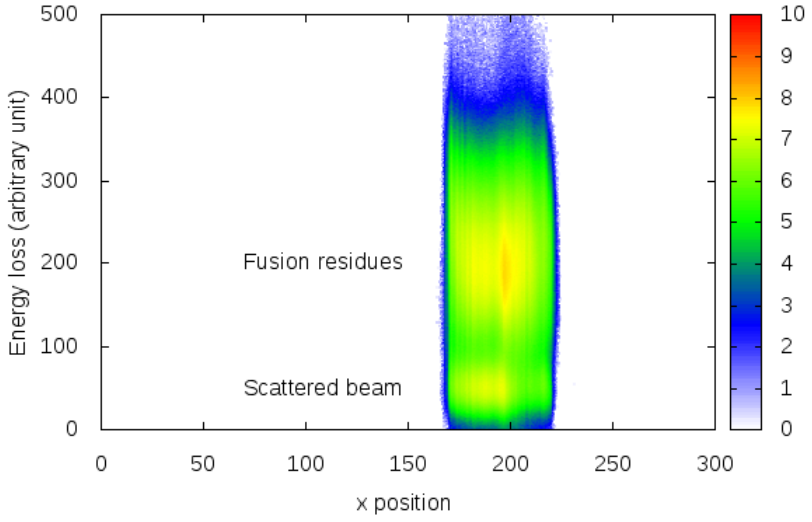

Figure 3.6: Energy loss of ions passing through the MWPC versus horizontal position of ions. The sharp cut at the two edges of the distribution indicates that the slits eliminate unwanted A/Q components of recoils which do not include $A = 113$.

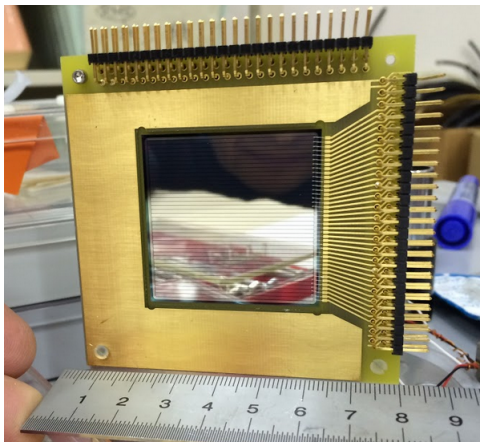

Figure 3.7: The DSSD used in this experiment. The rear side is showed in this figure.

highly intensive beams. Additionally, the area of the DSSD hit by the recoiling ions is enlarged by a factor of 1.41, reducing the count rate in the center pixels.

The count rate of DSSD varies with the position. For ions, the count rate is measured to be 16.2 cps and 2.2 cps for the center and border pixels. For decays, the values are 0.1 cps and 0.04 cps respectively.

3.4.3 Si-PIN detector

Two Si-PIN detectors at the thickness of 500 μm were used to suppress escaping decay products (α-particles/protons) from DSSD. They are sensitive to beta-particles as well. One of them is placed right behind the DSSD while the other one, kept parallel to the direction of the beam, is placed opposite to DSSD. α-particles and protons emitted by nuclei were expected to be stopped inside the DSSD, thus releasing all their energy there. As mentioned above, the shallow implantation depth in DSSD of recoiling ions makes it easy for emitted charged particles to escape. This will be discussed in details in Chapter 4. The count rate was 62.3 cps on front Si-PIN detector and 1.92×10^3 cps on back Si-PIN.

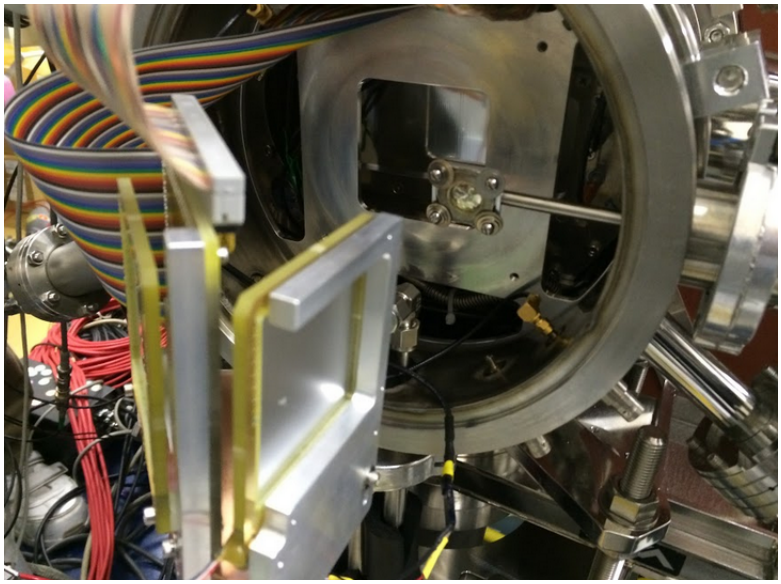

Figure 3.8: Implantation detectors DSSD, Si-PIN detectors assembled together, viewed from down stream.

3.4.4 NaI detector

A set of high-efficiency gamma-ray detectors, NaI array, was placed around the DSSD. This array is composed of a barrel like crystal segmented into 4 parts and a cylinder like crystal as the plug part. Four photomultiplier tubes (PMT) are connected to the end of the plug crystal and two PMTs are connected to each segment of the barrel part (see Figure 3.9).

In this experiment, the most abundant isobaric contaminants are all $\beta+$/EC decaying and some of them like ^{113}Xe are beta delayed proton precursors which produce a broad decay background in DSSD. This makes it difficult to identify α-particles or direct protons among them. Most of the time, β-delayed particle emission is associated with positron emission and its subsequent annihilation into two 511 keV photons, except for the small EC branches. This NaI array, covering more than half of the solid angle around the implantation chamber, is able to suppress such background by catching 511 keV photons propagating in opposite direction. The NaI array worked together with the Si-PIN detectors as veto for beta-decaying contaminants. It can also be utilized to search for beta-decay branch of ^{113}Ba.

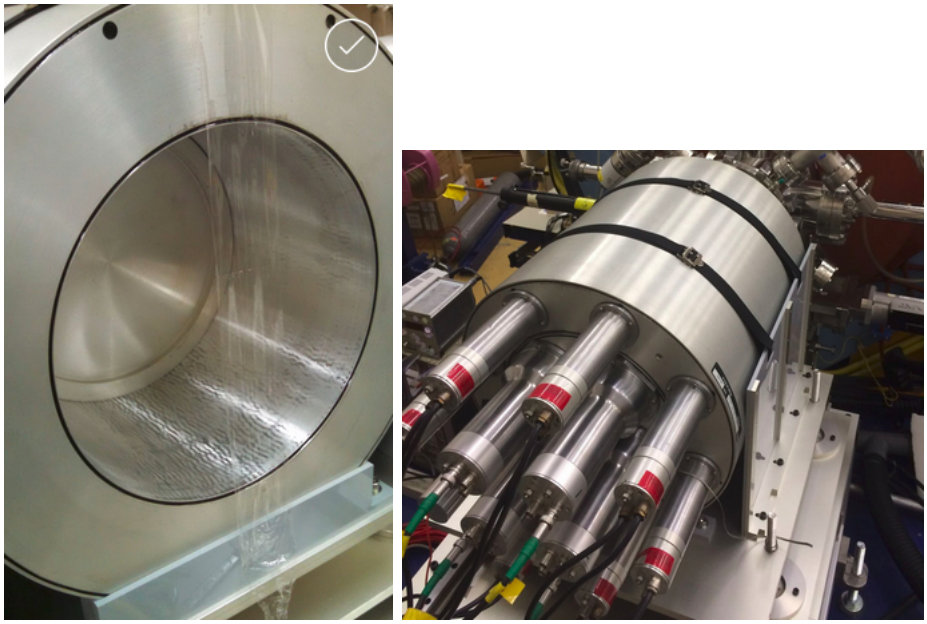

Figure 3.9: On the left is a view on NaI array from the front side. The implantation is placed into the concave by the array thus half of the solid angle around it is surrounded by the array. On the right is the NaI array viewed from the rear.

3.5 Digital Data Acquisition System

Data from all detectors were collected by digital data acquisition system Pixie-16 [41]. Output from pre-amplifiers were directly sent to Pixie-16 modules. For each event, time stamp and amplitude was assigned by applying on-board digital trapezoidal energy and timing filter to the signal pulse. The details of principles are explained below.

In Pixie-16, FPGA implemented are two digital trapezoidal filters. One is the energy filter (slow filter) with long rise time and gap time and the other one is the trigger filter (fast filter) with much shorter rise time and zero-gap time. The pulse from pre-amplifiers will first be digitized by the analogue-to-digital converter (ADC) and then transformed digitally by these two filters. A threshold is pre-set by the user for the trigger filter. When the output from the trigger filter goes beyond this threshold, the crossing point will be taken as the arrival of a pulse. The height of the flat top of the output by energy filter will then be evaluated therefore the energy of the pulse is determined (see Figure 3.10[41]).

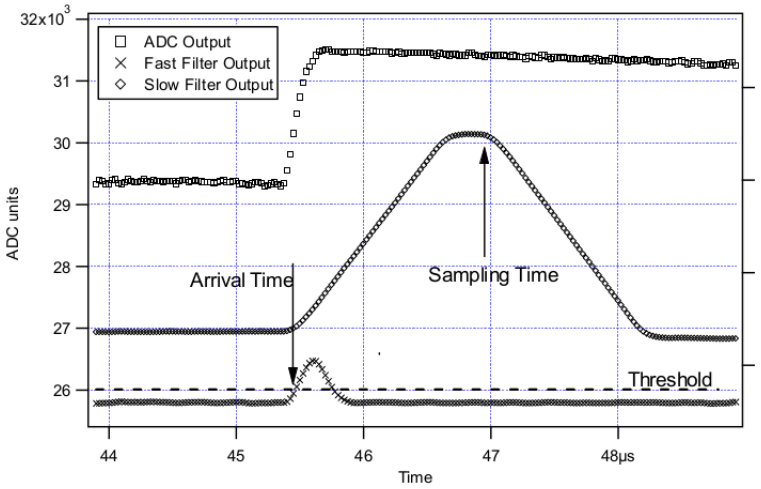

Figure 3.10: The principles of digital trapezoidal filters and how the timing and energy of a pulse is determined.

In the offline software and analysis of the data, ion-decay events were reconstructed by spatial and temporal correlation techniques. A real time signal processing algorithm for pile-up detection was implemented in this experiment [42]. Once a pile-up signal is detected, on one hand, the pulse height returned by the on-board analyser is saved, while on the other hand, the pile-up pulse shape (trace) was recorded for further analysis. All saved traces are 10 μs in length and the recording starts from 2 μs prior to the leading edge of the first pulse.

New correlation features were added into the offline code so that correlation or anti-correlation between DSSD and other detectors can be made. In particular, the multi-generation correlation analysis for decay chain analysis were implemented up to 3^{th} generation for DSSD signals. The details will be explained in following chapters.

Chapter 4

Data Analysis

4.1 Proof-of-principle Experiment

In order to test the capability of the JAEA RMS and the detection system, a proof-of-principle experiment was performed in March, 2014. The isotope ^{109}Xe was expected to be produced via the fusion-evaporation reaction ^{54}Fe(^{58}Ni, 2n)^{109}Xe, similar to the original experiment carried out in HRIBF, Oak Ridge National Laboratory [20, 21]. The detector set-up was similar to the later configuration for ^{113}Ba experiment augumented by the two Si-PIN detectors and the NaI detection array.

Four pile-up traces of decay chain were observed (see Fig.4.1). This is an indication that our fast digital data acquisition system and the pile-up inspector implemented in the offline analysis code were able to detect pile-up signals within very short time interval.

The measurement of the energies of the first and α-particles potentially emitted by ^{109}Xe and ^{105}Te is given in the Table 4.1. By comparing it to the previously measured values (see Figure 4.2 [21]), it can be concluded that all of these four transitions correspond to the ground-state to ground-state ($7/2^+ \rightarrow 5/2^+$) transition from ^{109}Xe with $b_\alpha = 69(7)\%$ succeeded by ground-state to excited state ($5/2^+ \rightarrow 5/2^+$) transition from ^{105}Te. The difference in energy is within the energy resolution of DSSD ($\sim$1.4%).

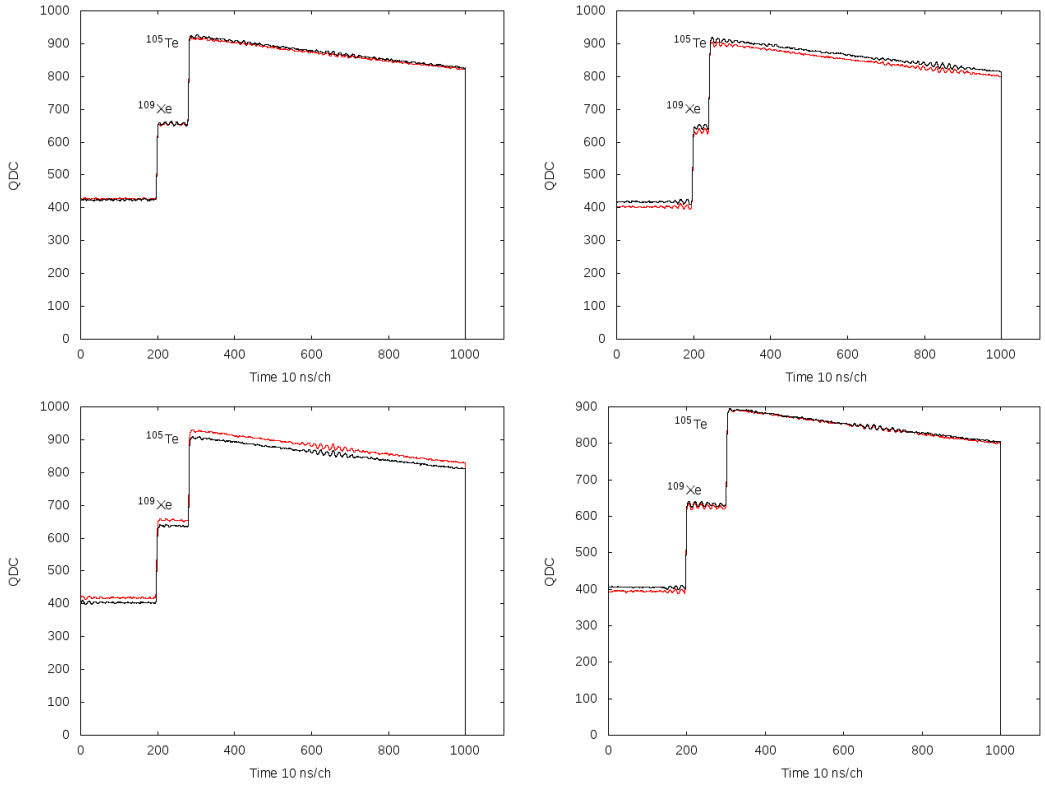

Figure 4.1: Four raw pile-up traces of decay chain ^{109}Xe $\rightarrow$ ^{105}Te $\rightarrow$ ^{101}Sn found in the proof-of-principle experiment. The red and blue traces are recorded by front and back side of DSSD respectively.

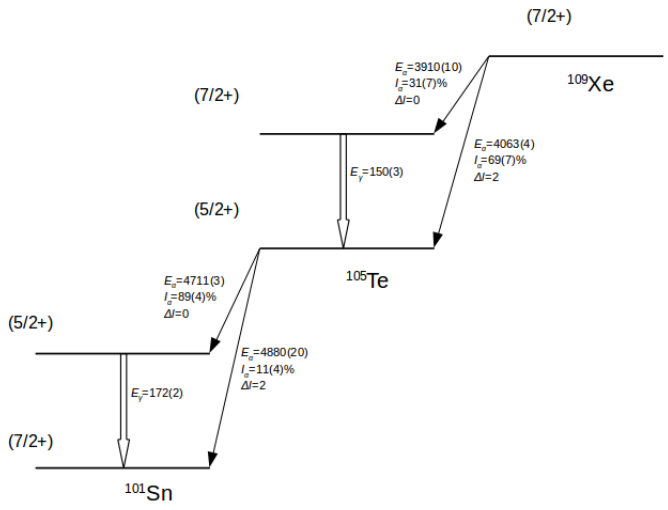

Figure 4.2: Paths of α-decay chain ^{109}Xe $\rightarrow$ ^{105}Te $\rightarrow$ ^{101}Sn. Energies are shown in the unit of keV.

Table 4.1: Details of recorded four pile-up traces in the proof-of-principle experiment. Δt_1 is the time difference between the first α-particle and the preceding ion implantation in the same pixel. Δt_2 is the time difference between the two α-particles. $E_{\alpha,1,2}$ are the recorded energies of α-particle by DSSD averaged over front and back values.

Trace Num.	Δt_1(ms)	$E_{\alpha,1}$(keV)	$\Delta t_2(\mu$s)	$E_{\alpha,2}$(keV)
1	39.95	4009	0.83	4603
2	14.37	3998	0.43	4610
3	10.21	4030	0.82	4615
4	8.47	4021	1.03	4587

The two group of time intervals Δt_1 and Δt_2 were analysed and compared to the previously determined half-lives of ^{109}Xe and ^{105}Te. Usually, in the analysis for radioactive decay data, the time difference between consequent decay events are filled into time intervals with constant width Δt which results in the exponential decay curve in linear time scale. This method, however, is not appropriate in the case of low statistics. There are many time bins without a single count and the shape of the spectrum is subject to random fluctuations.

It is proposed by Schmidt *et al* [43] that in case of poor statistics, one can sort the radioactive data into a spectrum with time intervals Δt which has $\Delta t/t$=constant. This method enables the storage of decays over a very large range of times with a reasonable number of bins. The corresponding distribution is given by:

$$\frac{dn}{dln(t)} = \frac{dn}{dt}\frac{dt}{dln(t)} = -n_0\lambda e^{-\lambda t} \tag{4.1}$$

If one defines: $\Theta = ln(t)$, then:

$$\mid \frac{dn}{d\Theta} \mid = n_0 \cdot \lambda e^{\Theta} \cdot e^{-\lambda e^{\Theta}} \tag{4.2}$$

The resulted slightly asymmetric, bell-shaped curve does not dependent on the decay constant λ and thus is in a universal shape. The maximum of the function is at Θ_{max} where:

$$\frac{d^2n}{d\Theta^2} = 0 \rightarrow \Theta_{max} = ln(\frac{1}{\lambda}). \tag{4.3}$$

The standard deviation σ_Θ is about 1.28 with a lower and upper limit depending on the size of total statistics [44]. If the experimentally measured standard deviation falls outside the lower limit, it might be an indication that the decay time spectrum is not complete. If this is not the case, the observed events do not originate from radioactive decays but some other sources.

The distribution of Δt_1 of the four pile-up events are plotted in logarithmic time scale as mentioned above (see Figure 4.3). The standard deviation σ_Θ is 0.58 falling between the lower limit 0.31 and the upper limit 1.92 for four events, while the expected value is 0.98. The returned value for λ is 46.6 s^{-1}, which corresponds to $T_{1/2}$=14.9±7.4 ms. This is in agreement with the previously determined $T_{1/2}$=13(2) ms for ^{109}Xe.

For Δt_2 between the first and second pulse, the distribution in logarithmic scale is shown in Figure 4.4). From the fit on Δt_2, the standard deviation σ_Θ is 0.33, slightly above the lower limit 0.31. The fitted value for λ=1.36×10^6 s^{-1} corresponds to $T_{1/2}$=0.51±0.26 μs. This is very close to the known $T_{1/2}$=0.62(7) μs for ^{105}Te.

Thus, it is confirmed that these four pile-up traces correspond to the ^{109}Xe → ^{105}Te → ^{101}Sn decay chain. The reaction cross section of ^{109}Xe was measured as low as 20 nb at the energy of 250 MeV of primary beam. It was the third observation of alpha-decay of ^{109}Xe and a proof that the RMS is capable for ^{113}Ba search experiment with very low cross section.

4.2 ^{113}Ba Experiment

4.2.1 Performance of Detectors

DSSD

The calibration of DSSD is based on the assumption that the response of the DSSD is linear to the energy deposited by charged particles and that the induced charges collected by the front and back strip should be similar within the energy resolution of DSSD. The energy region of interest in this experiment ranges from several hundred keV for protons up to 5

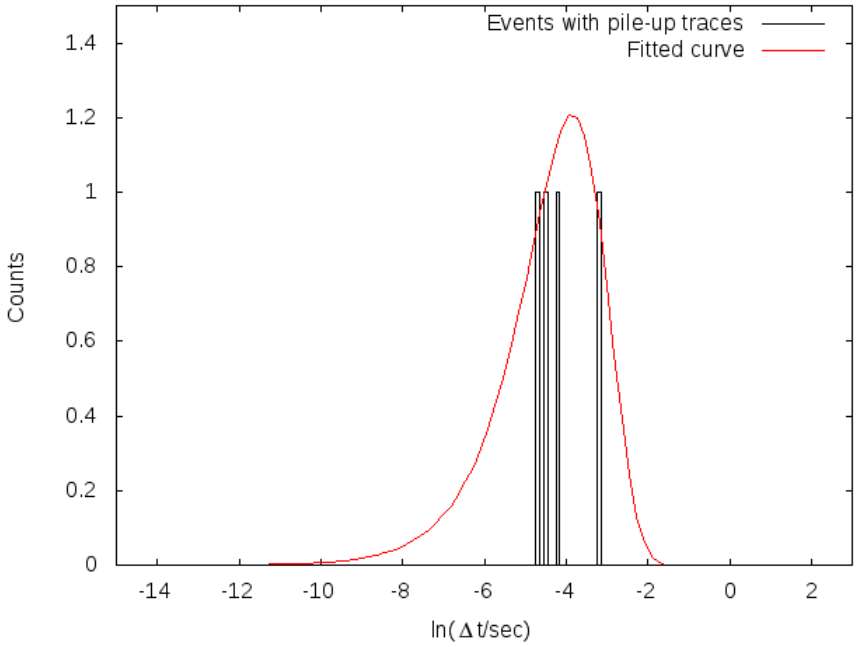

Figure 4.3: In red are distributions of Δt_1 for the four events recorded as pile-up signals and the red curve is the fit function.

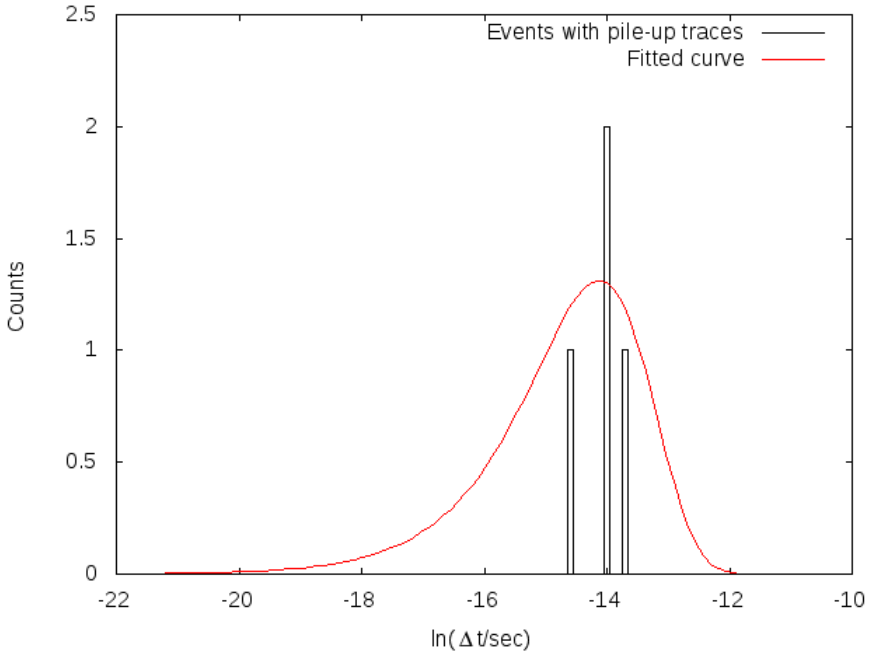

Figure 4.4: In red are distributions of Δt_2 for the four events recorded as pile-up signals and the green curve is the fit function.

MeV for α-particles. The calibration was made based on the proton line of ^{113}Cs at 965 keV and the most abundant α-decaying contaminant ^{109}Te with α-particle energy $E_\alpha = 3081$ keV. For each of the total 80 strips of the DSSD front and back the calibration procedure is done iteratively with the input data for several times with minor adjustments to the parameters each time and finally determined the optimum values. The calibrated decay spectrum of DSSD vs front strip position is shown below in Figure 4.5. The energy resolution of the DSSD based on the calibration is calculated to be 5.2 % for 965 keV proton line of ^{113}Cs and 1.4 % for 3107 keV α-line of ^{109}Te (see Figure 4.6).

It is necessary to be noted that for pile-up signals in this experiment, only the pulse shape (traces) will be recorded. Energies and time stamps with respective to the leading signal are to deduced by the digital trapezoidal filter implemented in the offline scan code instead of the on-board filter. Therefore, the consistency between these two deduced energies is required. In order to achieve this goal, one of the data run with ^{241}Am source with the function of recording traces enabled was used to test the capability of parameters of the energy trapezoidal filters as well as the contraction coefficient between on-board filter and offline filter to reproduce the correct energy from recorded trace. These values were corrected according to the comparison between the already-known α-particle energy of ^{241}Am and filtered out values.

One of the main issues associated with the performance of DSSD is the probability of recording full energy of detected changed particles which is a function of penetration of recoiling ions and projected range of charged particles.

As mentioned above, energies of incoming ions passing through the MWPC at focal plane range from 37.5 MeV to 50 MeV based on extrapolation from decay spectrum of DSSD with same calibration. The relation among energy implantation depth, normal with respect to the front surface of DSSD, projected range and detection probability are calculated by the stopping and range of ions in matter (SRIM) code [45] and listed in Table 4.2.

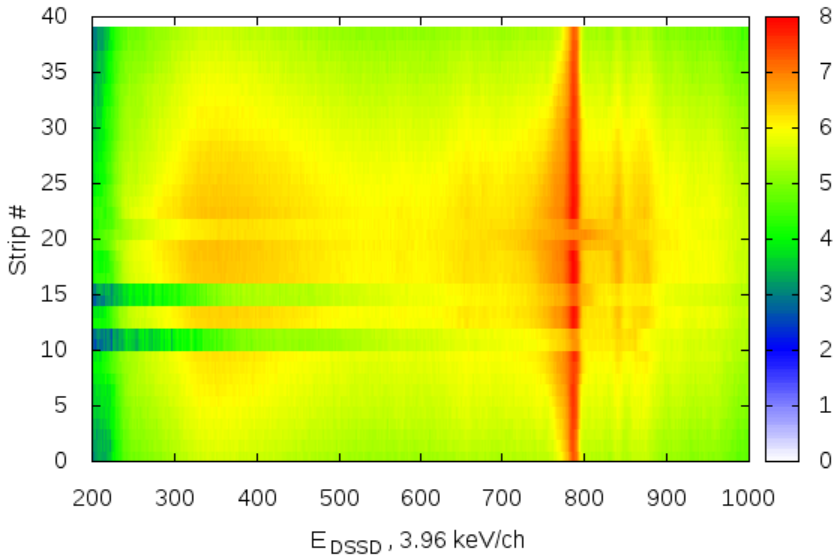

Figure 4.5: Calibrated spectrum of energy of decays in DSSD versus the front strip position. The α-peak of ^{109}Te on different strips are now aligned well. The possible reason for the loss of enough statistics on certain strips might be the radiation damage on these strips.

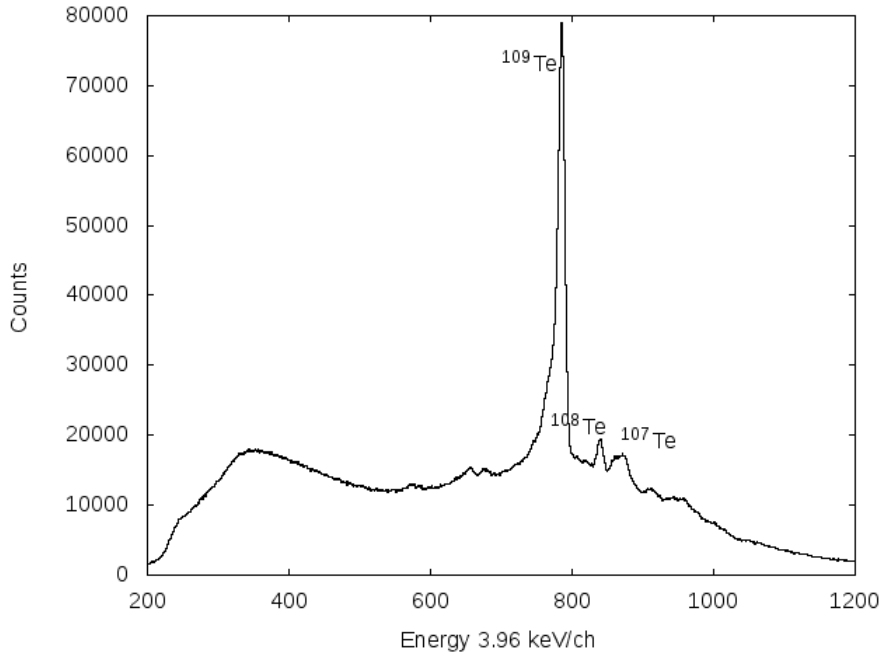

Figure 4.6: A portion of calibrated decay spectrum of DSSD, projected from Figure 4.5 above. The three most evident α-decay peaks belong to ^{109,108,107}Te respectively.

Table 4.2: Table of ion energies, implantation depth and probability P for full alpha-particle energy deposition. E_{imp} is the energy of implanted ions at the focal plane of the RMS. D_{imp} is the implantation depth of an ion in silicon. N is the distance between the front surface of DSSD and where it is stopped.

E_{imp}(keV)	D_{imp}(μm)	N(μm)	Emitter	P(%)
37500	8.93	5.93	^{113}Ba	53.1
			^{109}Xe	52.8
			^{105}Te	51.8
40000	8.75	6.19	^{113}Ba	53.4
			^{109}Xe	53.0
			^{105}Te	51.9
42000	9.03	6.38	^{113}Ba	53.7
			^{109}Xe	53.2
			^{105}Te	52.1
44000	9.43	6.67	^{113}Ba	54.0
			^{109}Xe	53.6
			^{105}Te	52.3
46000	9.57	6.77	^{113}Ba	54.1
			^{109}Xe	53.7
			^{105}Te	52.3
48000	9.83	6.95	^{113}Ba	54.4
			^{109}Xe	53.9
			^{105}Te	52.5

Table 4.3: Correspondence between alpha-particle energy and range in silicon.

Mother Nucleus	E_α(keV)	$R_\alpha(\mu$m)
^{113}Ba	3877.7	17.01
^{109}Xe	4063.0	18.01
^{105}Te	4711	22.38

The probability of recording full energy of a charged particle as a function of the depth where its mother nucleus is implanted and its projected range in silicon is given below:

$$P = 1 - \frac{1}{2}\sqrt{1 - (\frac{N}{R_\alpha})^2} \tag{4.4}$$

where R_α is the projected range of an α-particle in silicon, N is the normal as mentioned above. The values for R_α are calculated by SRIM and listed in Table 4.3, where kinetic energies of α-particles are calculated based on the simple relation $E_\alpha = Q_\alpha \times (A-4)/A$ correcting recoil effects and A is the mass number of the mother nucleus.

Once a charged particle escapes from the DSSD, first, it has to pass through the aluminized conductive layer. In this layer, the energy lost by the charged particle will not be measured, which effectively becomes a missing fraction of the energy of this particle. This value can be evaluated by the difference in measured energy of α-particles emitted by ^{109}Te and that of ^{241}Am since in the latter case, the α-particles have to come through the dead layer before getting registered inside DSSD while α-particles emitted by ^{109}Te are from the inside. In this way, the effective energy loss in the front and back dead layer of DSSD is evaluated to be 211 keV and 227 keV.

NaI

The calibration for NaI detection array are made separately for the plug-in and barrel part. For the plug-in part, in the first step, the four independent channels are gain-matched by using ^{137}Cs source with γ-line at 662 keV so that the full energy photo peak delivered by these four channels are aligned well. In the second step, the signals from the four PMTs are summed together within a given event of 0.5 μs, which gives the total energy of a photon

deposited into the barrel crystal. It is again assumed that the response of the NaI scintillator is linear with the energy of γ-rays. The calibration is therefore made with two already known γ-lines, the 662 keV line of ^{137}Cs and the 1173 keV line of ^{60}Co (see Figure 4.7).

For the barrel part, since the crystal is segmented into four parts, summed signals collected from two PMTs attached to each segmentation will be processed independently. The calibration was made with the double γ-lines at 1173 keV and 1332 keV of ^{60}Co source and verified with the ^{137}Cs source. The threshold of the barrel part of this detector is around 600 keV which makes it impossible to see 511 keV photons from positron-electron annihilation but also for the detection of the fine structure of α-decay of ^{109}Xe and ^{105}Te (see Figure 4.8). This issue makes the efficiency of veto on β^+-decay much lower than expected since much less solid angle around the implantation chamber is now covered by the NaI detection array.

The energy resolution of the plug-in part of NaI detection array is 11.2 % at 662 keV. The detection efficiency of it for 511 keV can be estimated from the detection for 662 keV γ-ray of the ^{137}Cs source with calibrated activity upon the assumption of similar behaviour of the detector. Note that the two 511 keV photons resulted from positron-electron annihilation always propagate in opposite direction. The veto efficiency of the NaI array for β^+-decay should be twice as high as that for seeing 662 keV photons. The calculated result is 12.5 %.

Si-PIN

The calibration of Si-PIN detectors is made with ^{241}Am source with primary α-line at 5485.6 keV and branching ratio of 84.8(5)% (see Figure 4.9). The energy resolution of the front and back ones are 3.2 % and 1.1% at 5485.6 keV respectively.

As mentioned above, the Si-PIN detectors are used as veto detectors to record escaping α-particles, protons or positrons escaping from DSSD. Shown in the blue and green profile of Figure 4.9 is the energy distribution of signals in Si-PIN during experiment. To understand different components, one has to make a spectrum displaying signals in coincidence between two Si-PIN detectors and two sides of DSSD respectively.

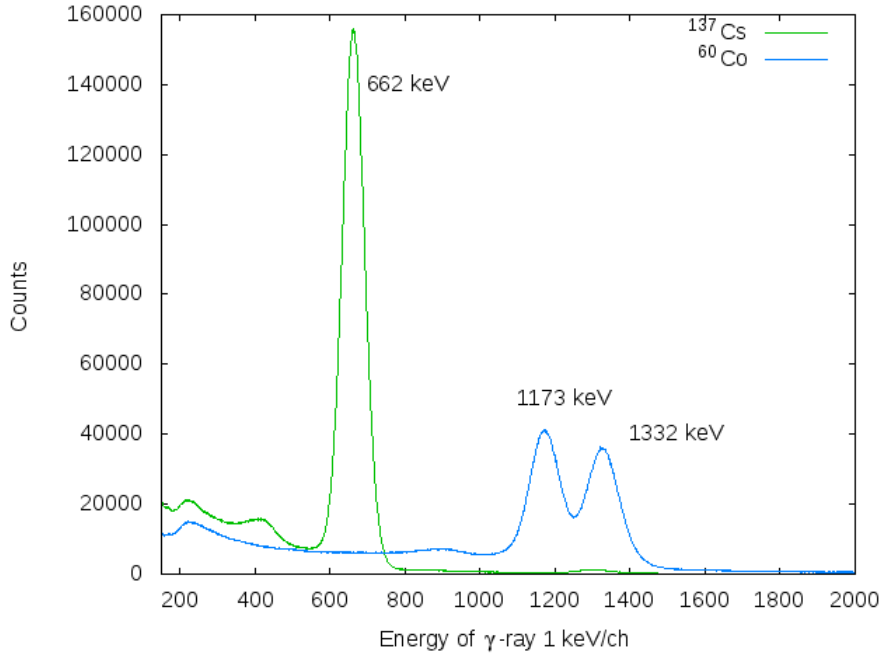

Figure 4.7: Calibrated plug-in NaI crystal spectrum with ^{137}Cs and ^{60}Co γ-source.

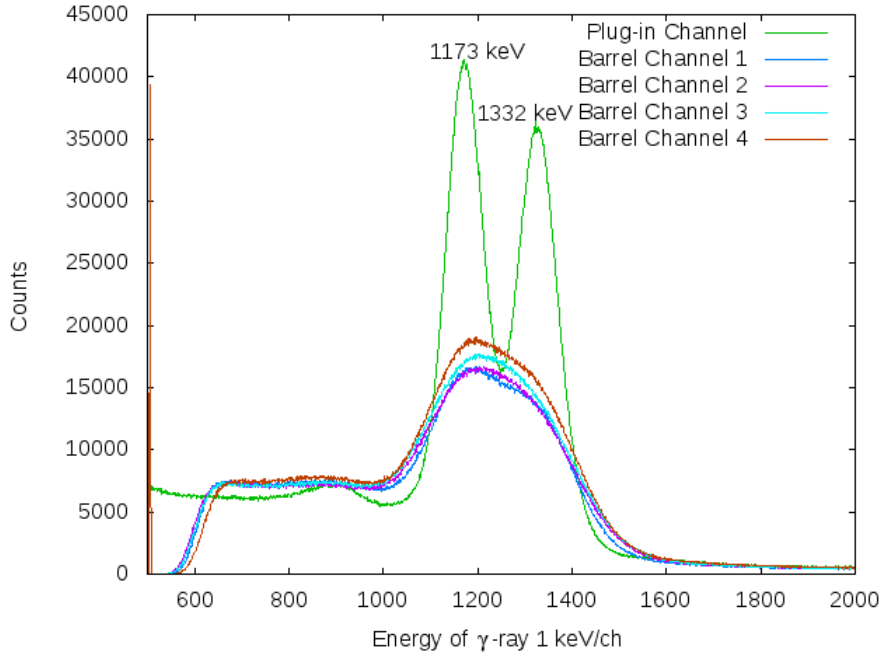

Figure 4.8: Comparison between γ-spectrum measured with ^{60}Co source by plug-in part and barrel part of NaI detection array. The threshold in the barrel channels are around 600 keV which is too high to make the barrel part efficiently veto 511 keV γ-rays.

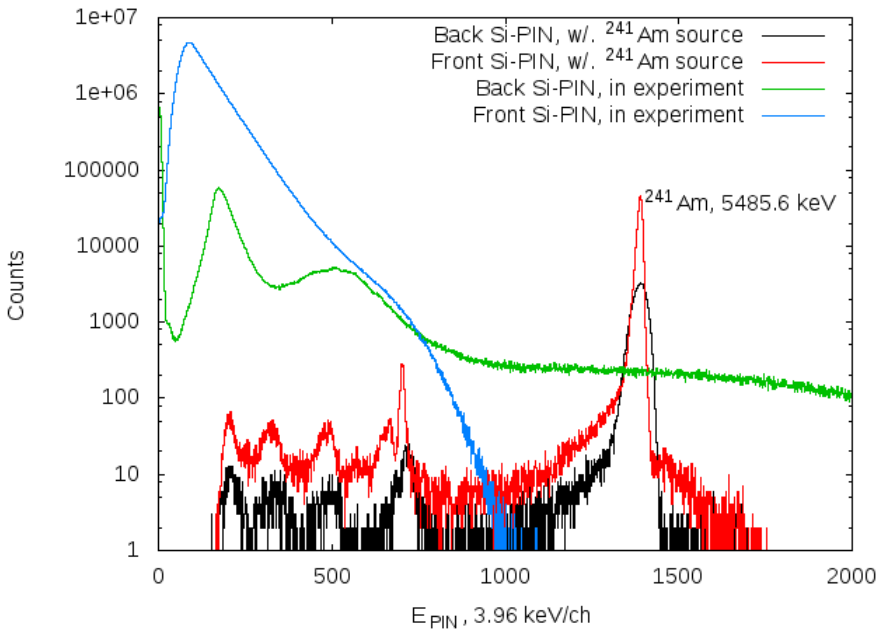

Figure 4.9: Calibrated spectra of front and back Si-PIN detectors measured with ^{241}Am source and measured in experiments.

In Figure 4.10, the most evident line on the left corresponds to α-particles emitted by ^{109}Te which escaped from DSSD and then registered in the front Si-PIN. The projection of this spectrum onto the y-axis and its comparison with the energy spectrum in the front Si-PIN suggest that the majority of the front Si-PIN spectrum is consisted of escaping α-particles and the overwhelming β-delayed protons which contribute greatly in decay spectrum of DSSD as well. The situation for the coincidence spectrum between the back Si-PIN and the back side of DSSD is similar except that α-particles from tellurium isotopes are not energetic enough to penetrate the 65 μm-thick DSSD. The dominance of β-delayed protons in spectra of Si-PIN detector is supported by the calculation made with SRIM (see Figure 4.12).

An interesting question is whether it is possible or not to directly detect positrons in DSSD or Si-PIN which might be used as triggers when the detection efficiency of detecting 511 keV photons is low. The distribution of positrons in silicon is a function of the ratio z/r_0 where r_0 is the average range of a positron and z is the thickness of the silicon bulk.

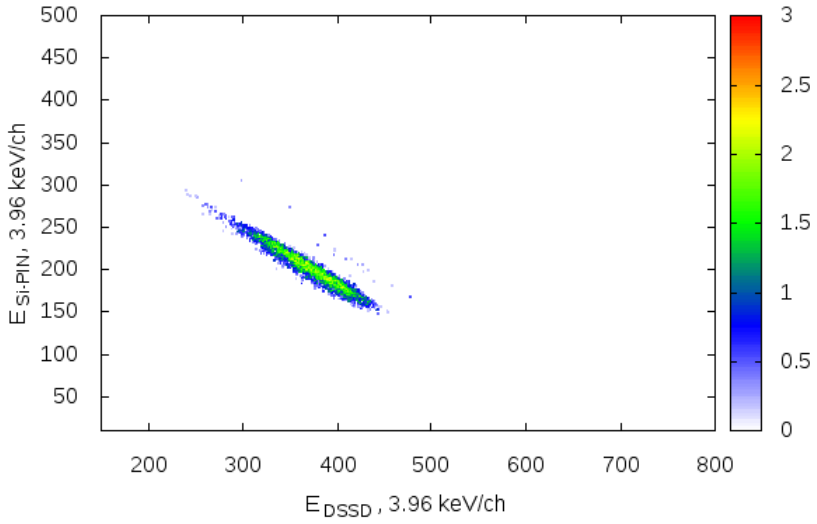

Figure 4.10: Coincident signals between DSSD and the front Si-PIN detector. The most evident line corresponds to α-particles emitted by ^{109}Te which escaped from DSSD and then registered in the front Si-PIN.

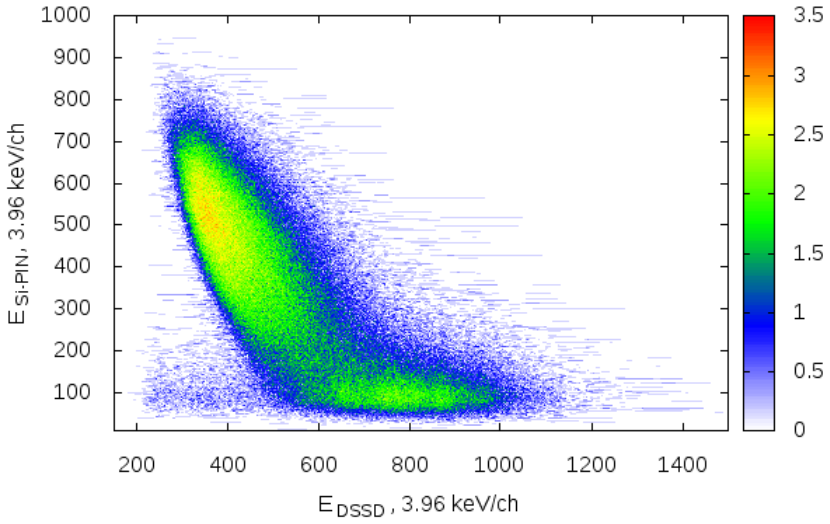

Figure 4.11: Coincident signals between DSSD and the back Si-PIN detector. This spectrum is fully filled with β-delayed protons passing through the DSSD backward and registered in Si-PIN detector.

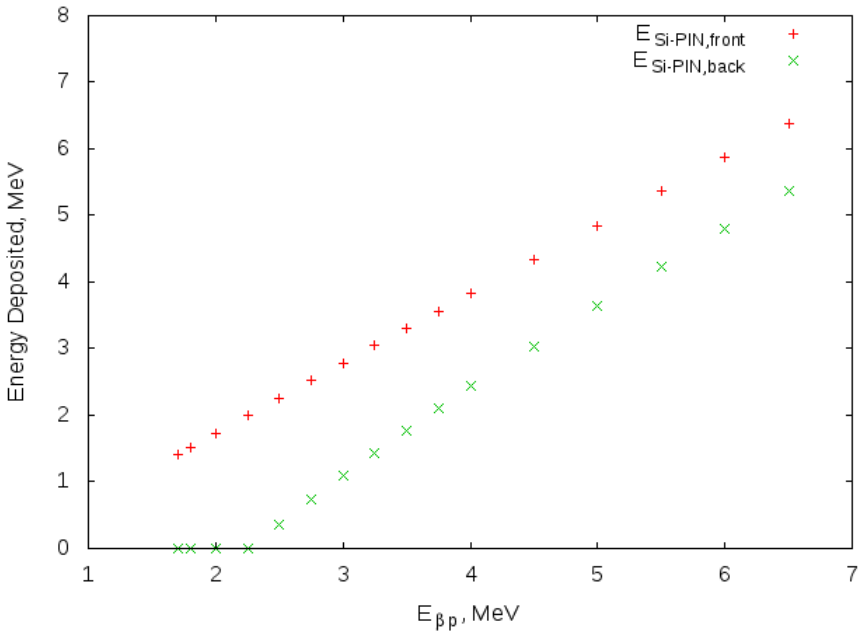

Figure 4.12: Calculation of energy deposition of β-delayed protons in Si-PIN detectors. The $E_{front,PIN}, E_{back,PIN}$ are the maximum energy can be left by particles in the front/back Si-PIN detector, corresponding particles emitted forward and backward. The range for typical energies of β-delayed protons were covered for βp-emitters in the region above ^{100}Sn.

Table 4.4: CSDA range for positrons and their stopping power. The last column gives the ratio of thickness of the silicon bulk (500 μm for Si-PIN) to the CSDA range of a positron, which determines the shape of energy distribution of β-particles in silicon. See next section for details.

K.E.$_{e^+}$ (MeV)	SP$_{Si}$(MeV/μm)	CSDA range(g/cm^2)	Range(μm)	z/r_0
4	3.94×10^{-4}	2.41	1.04×10^{4}	4.8×10^{-2}
5	4.08×10^{-4}	2.99	1.29×10^{4}	3.87×10^{-2}
6	4.20×10^{-4}	3.55	1.53×10^{4}	3.26×10^{-2}
7	4.33×10^{-4}	4.10	1.76×10^{4}	2.84×10^{-2}
8	4.44×10^{-4}	4.62	1.99×10^{4}	2.51×10^{-2}
9	4.55×10^{-4}	5.14	2.22×10^{4}	2.25×10^{-2}
10	4.67×10^{-4}	5.64	2.43×10^{4}	2.05×10^{-2}
12.5	4.94×10^{-4}	6.85	2.95×10^{4}	1.69×10^{-2}

For positrons with kinetic energy above 1 MeV, the distribution is shown in Figure 4.13 [46] corresponding to different z/r_0 values.

The extrapolated Q_{EC} of ^{113}Ba from its neighbouring nuclei is 12 MeV. Thus, for the energy distribution of positrons, the largest probability lies at 6 MeV. A calculation was made with stopping powers and ranges for electrons (ESTAR) calculator provided by NIST [47] to figure out the continuously slowing down approximation (CSDA) range of positrons in silicon and corresponding z/r_0 values as well. The results are given in Table 4.4. In cases above, the z/r_0 ratio is closest to the top right subfigure in Figure 4.13. It is then straight forward to explain the small decreasing component at the very left of experiment spectrum of front Si-PIN in Figure 4.9 as positrons. Unfortunately there is no counter part in the spectrum of back Si-PIN. The only distinguishable energy distribution of positrons in the front Si-PIN are not displayed in full in comparison with Figure 4.13 and the spreading energy distribution makes things even more complicated compared to distributions of mono energy. Thus, it is not realistic to rely on Si-PIN to efficiently record fingerprints of β-decays.

4.2.2 α-decay Branch

The main idea to identify the nucleus ^{113}Ba among the fusion-evaporation products is to exploit its alpha-decay chain $^{113}\text{Ba} \rightarrow {}^{109}\text{Xe} \rightarrow {}^{105}\text{Te} \rightarrow {}^{101}\text{Sn}$ which will provide a unique

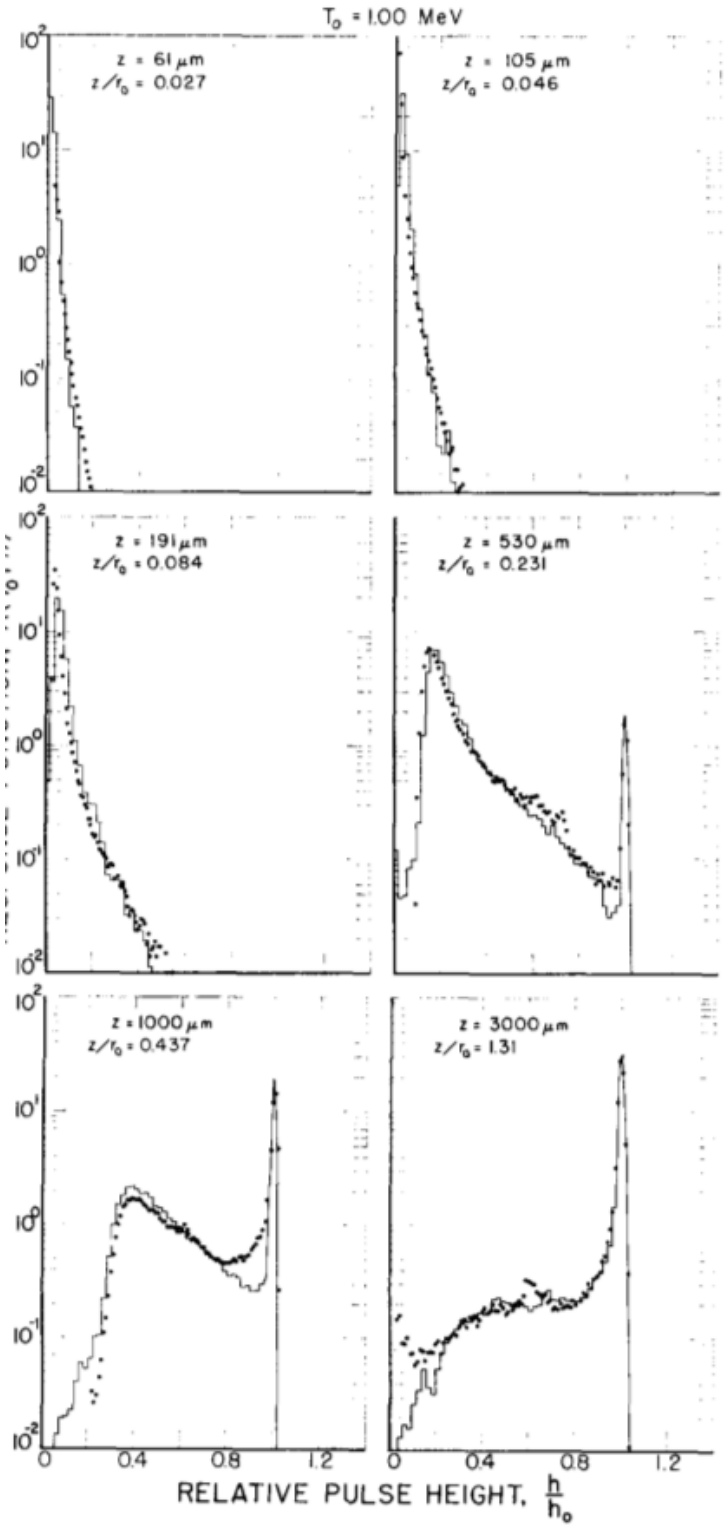

Figure 4.13: Behaviour of electrons with kinetic energy of 1 MeV in bulk silicon with different thickness. For electrons with energy up to 5 MeV, the shape of the distribution is very similar.

signature. The capabilities were used to search for this decay path. The digital trapezoidal trigger and energy filters in the offline analysis code were adjusted so that closely spaced in time pile-up traces of decay chain ^{109}Xe $\rightarrow$ ^{105}Te $\rightarrow$ ^{101}Sn can be recorded with time interval between 200 ms and 8 μs. Once such double α-particle decay chain is found, a search for the preceding implantation of ion ^{113}Ba and its directly emitted alpha-particle is carried out. This method was originally developed and implemented in for the superheavy element research.

Decay Correlation Matrix

In order to search for the double α-decay chain within the collected data, a correlation matrix was set up searching for sequential α-decay events within very short time intervals. Before making correlations between signals, it is necessary to distinguish decay signals from ion implantations. This goal can be achieved by using energy information from the DSSD and the signal from the auxiliary MWPC detector.

As mentioned in previous section, the typical energy of incoming ions passing through the MWPC is around 40 MeV. Therefore, the time-of-flight from MWPC plane to DSSD is less than 50 ns which is much shorter than the length of an event 500 ns and is considered instantaneous with DSSD. If a signal is gated on MWPC within the same event where it is recorded in DSSD, it can be taken as an ion implantation, as long as the time difference between the time stamps of MWPC signal and the DSSD signal is less than 50 ns. The time stamp and the front/back strip energy will be recorded in the corresponding element of the matrix. In other cases, where a signal registered in DSSD with energy higher than 25 MeV, it will be taken as an ion.

If the energy of a non-implantation signal is less than 15 MeV and greater than 200 keV below which the noise become dominant, it can be considered as a decay. Additional conditions are that it should not be recorded by DSSD at the same time when there is any ion implantation in the adjacent eight pixels. This is due to the fact that charges may be induced by ions with much higher energy and they may spread across the border between two strips of DSSD, which is known as the "cross talk". The signal amplitude due to induced charge

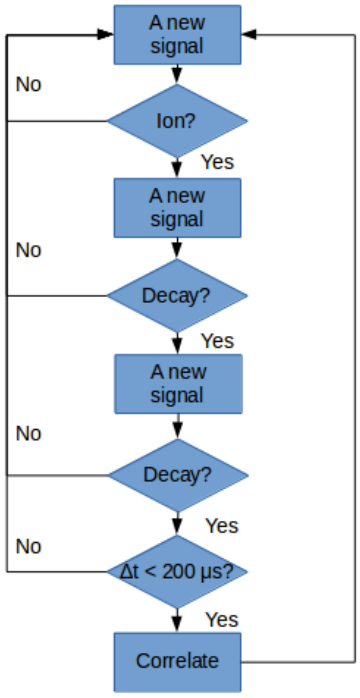

Figure 4.14: Flowchart of making correlation between two generations of decays.

detected by the neighbouring strip could be of the same order as for typical decays and this can be misleading in analysis. By adding this condition, such false decays are eliminated.

The correlation matrix is intended to find the two consecutive decays in the same pixel preceded by an ion implantation. Whenever there is an ion coming in, the information about the recorded decays is reset and successive decay signals can be recorded again (see flowchart in Figure 4.14). Once the correlation between the two decays are made, a location is marked inside the matrix with its x- and y-coordinates being the energy of the first and second signal. Then, the whole decay chain including the ion implantation and the two decays for the certain pixel are reset until a new ion comes in. An additional condition is applied on recording correlated decays that if the time interval between them is beyond 200 μs which is more than 200 times as long as the half-life $T_{1/2} = 0.62\mu$s of ^{105}Te, the whole decay chain will be reset as well. In this way, decay chains involving nucleus with much longer life time or unwanted random decays will be eliminated (see Figure 4.15). In the lower panel of Figure

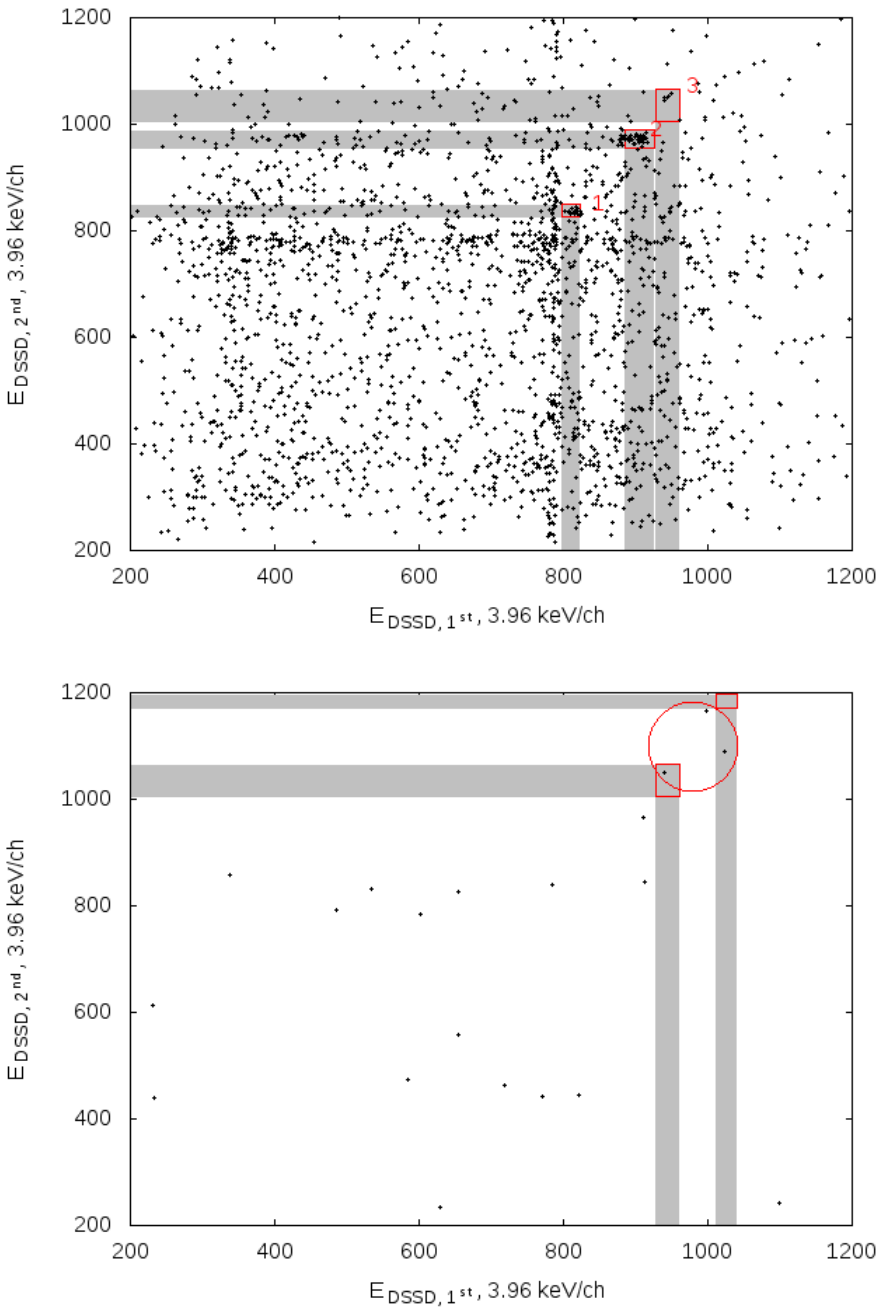

Figure 4.15: Comparison between correlation matrix with time window of 30 ms (upper) and 200 μs (lower). Shaded areas are expected energy range for the first and second signals in correlation successively. The overlapping region of two bands are the zones of interest for certain decay chains, enclosed by red rectangles. The first pile-up trace belongs to the decay chain ^{110}Xe $\rightarrow$ ^{106}Te $\rightarrow$ ^{102}Sn enclosed by rectangle 3 in the upper figure. The group 1 is the decay chain ^{112}Xe $\rightarrow$ ^{108}Te $\rightarrow$ ^{104}Sn and the group 2 is the decay chain ^{111}Xe $\rightarrow$ ^{107}Te $\rightarrow$ ^{103}Sn. In the red circle in the lower figure are the three pile-up signals in Table 4.5. The lower left one lies within the red rectangle 3 in the upper figure.

Table 4.5: Details of pile-up traces observed in experiment, where Δt_1 is the time interval between the leading pulse and the preceding ion in the same pixel, Δt_2 is the time difference between the pile-up pulses, $E_{1,2}$ are the energies of the first and the second pulse.

Trace Num.	Δt_1 (ms)	E_1 (keV)	Δt_2 (μs)	E_2 (keV)
1	26	3679±49	0.39	4158±57
2	72	3991±54	0.78	4617±63
3	2.7×10^2	4059±55	0.56	4320±58

4.15, there are three events identified in the region where the shortly spaced in time α-decays of ^{109}Xe and ^{105}Te are expected with time interval less than 200 μs.

Pile-up Traces

Three pile-up traces were observed in the experiment with expected pulse shape, consistent pulse height and time intervals front and back strips. The details are listed in Table 4.5. According to [21], the E_α and branching ratios of α-decay of ^{109}Xe are 4063(4) keV (69(7)%) and 3910 (10) keV (31(7)%). For α-decays of ^{105}Te, the values are 4880 (20) keV (11(4)%) and 4711 (3) keV (89(4)%). In comparison with these values, for the first pile-up trace (see Figure 4.16), the energy of both first and second pulse is more than 400 keV lower than what is expected for α-decay of ^{109}Xe and ^{105}Te. In contrast, it is consistent with the energy of α-decay of ^{110}Xe and ^{106}Te decay chain. The time interval between the first and second pulse is in agreement with the half-life $T_{1/2}$=0.62 μs for ^{109}Xe, however, much shorter than the known half-life $T_{1/2}$=70(17) μs for α-decay of ^{106}Te. Taking into account the isobaric contamination from the electro-magnetic separation process in the RMS, the direct production of ^{110}Xe surviving from the RMS and its subsequent α-decay chain is highly possible. By resetting the maximum time window Δt=30ms which is more than 400 times longer than $T_{1/2}$=70 μs for ^{106}Te, a new correlation matrix is produced where a small group of correlated decays ^{110}Xe $\rightarrow$ ^{106}Te $\rightarrow$ ^{102}Sn is visible (see counts encircled by the red circle 3 in Figure 4.15). The correlated decays to which the first pile-up trace corresponded is among this group.

For the second pile-up trace (see the upper panel in Figure 4.17), the measured values for energy of the first and second pulse are close to the previously determined values for

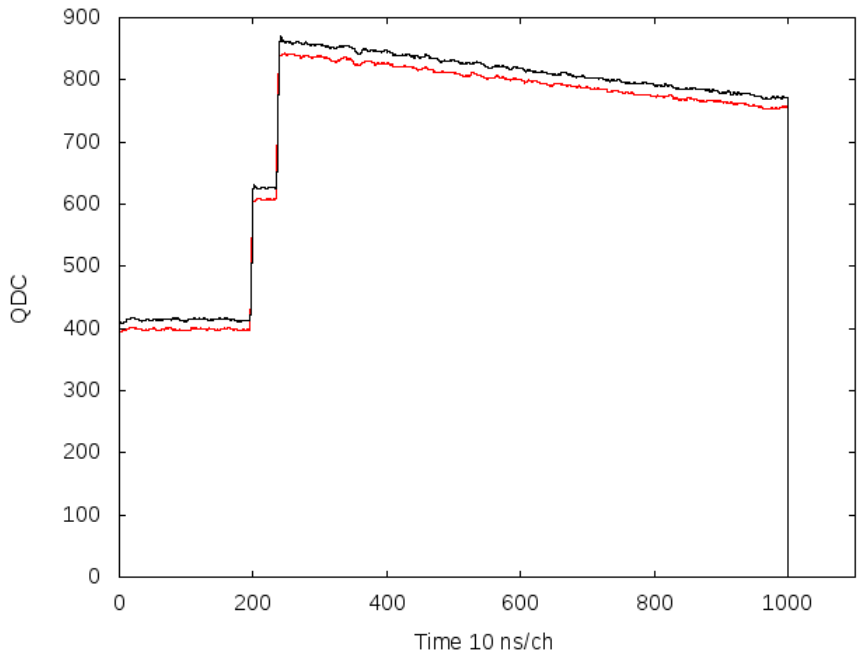

Figure 4.16: The first pile-up trace in Table 4.5. In black and red are the pulse shape recorded by the front and back side of DSSD.

^{109}Xe and ^{105}Te, only very slightly outside the margin of energy resolution of DSSD. The nearest implantation in time in the same pixel on DSSD was found 72.5 ms prior to this pile-up event. It is almost six times as long as the half-life $T_{1/2}$=13 ms of ^{109}Xe, leading to a probability less than 0.1 % of observing the direct production of ^{109}Xe and its subsequent α-decay.

The third pile-up trace (see the lower panel of Figure 4.17) was recorded with the two pulses at the energy of 4050 keV and 4317 keV. The latter value is more than 300 keV lower than what is known for the dominant ground-state to ground-state α-decay of ^{105}Te. The time difference between the preceding ion in the same pixel on DSSD is as long as 271.0 ms, making the probability of interpreting it as directly produced ^{109}Xe extremely small.

The fact that no α-particle was found between the leading pulse and the preceding local ion implantation may cause the doubt whether or not these two events were due to direct production of ^{109}Xe. Therefore, we refer to the fusion-evaporation code HIVAP [48, 49] for comparison between production cross section of ^{109}Xe via $\alpha 5n$ evaporation channel of ^{116}Ba

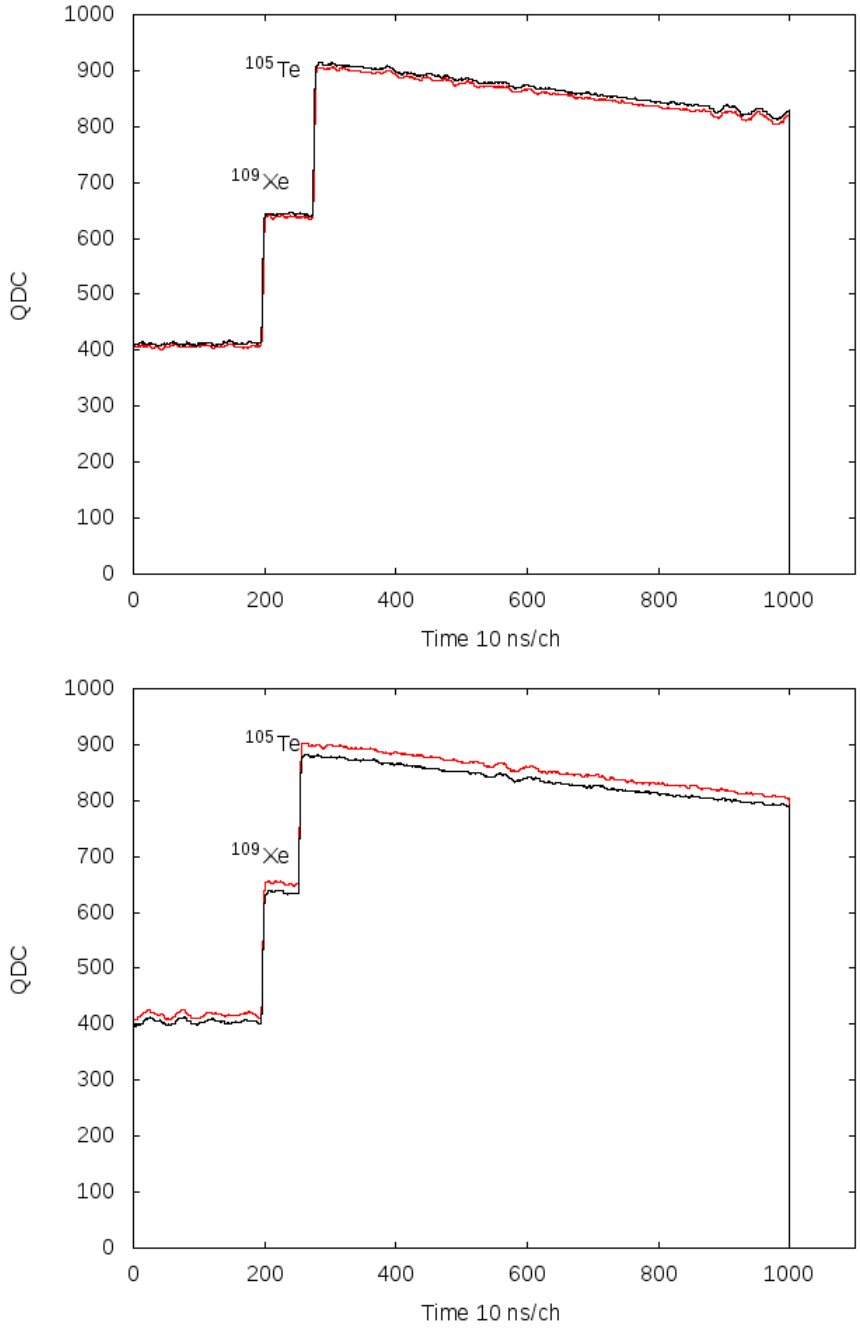

Figure 4.17: The second (upper) and third (lower) pile-up trace recorded with expected pulse shape and appropriate energy for α-decay for nucleus above ^{100}Sn region. Both are good candidates for the decay chain ^{109}Xe $\rightarrow$ ^{105}Te $\rightarrow$ ^{101}Sn which is expected to follow the α-decay of ^{113}Ba.

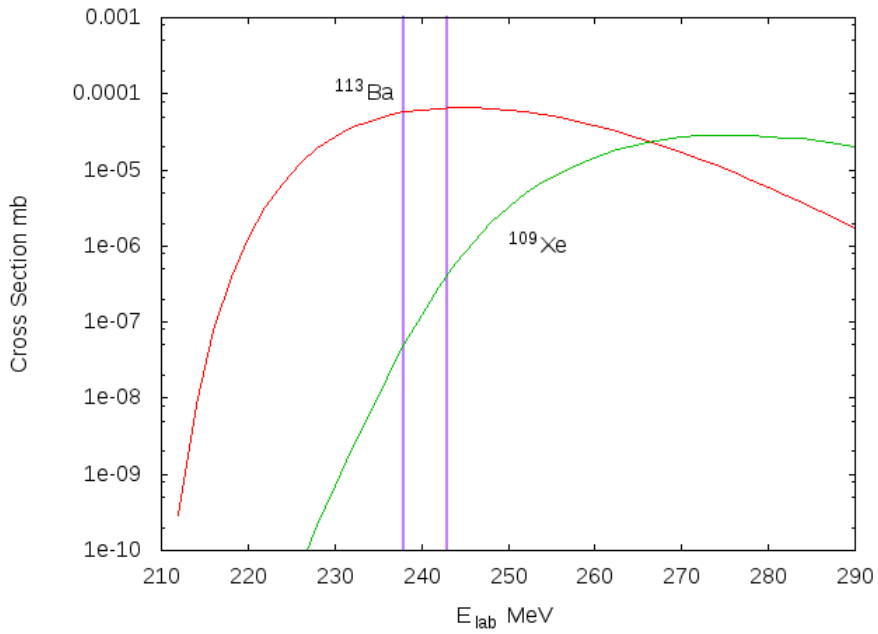

Figure 4.18: Comparison between production cross section of ^{109}Xe and ^{113}Ba. Two vertical lines indicate the effective energy of beam in the middle of thickness of the target at which the reaction took place.

and ^{113}Ba via $3n$ channel. When the beam hits the target, the energy loss of the beam passing through has to be taken into account. The energy loss of ^{58}Ni ions at the middle of the thickness of the 520 μg/cm^2 made of ^{58}Ni was 7.43 MeV while the energy of the primary beam was set to 245 MeV and 250 MeV. According to the calculation by HIVAP (see Figure 4.18), at the effective beam energy of 238 MeV, the reaction cross section for ^{113}Ba is 1145 times greater than that of ^{109}Xe. For higher effective beam energy of 243 MeV, this ratio comes down to 226. These calculations suggest that the probability of producing ^{109}Xe is hundreds of times smaller than that of ^{113}Ba at both energy settings in this experiment since the energy is not sufficient to evaporate the extra particles to produce ^{109}Xe. If the two pile-up trace were following direct production of ^{109}Xe instead of the α-decay of ^{113}Ba, many more ^{113}Ba events would have been observed.

Another argument can be made from the analysis on distribution of time intervals Δt_1 and Δt_2. In the first step, two values for Δt_2 above were put into logarithmic time scale. The standard deviation of the distribution of $ln(\Delta t_2)$ is 0.17, falling between the lower limit

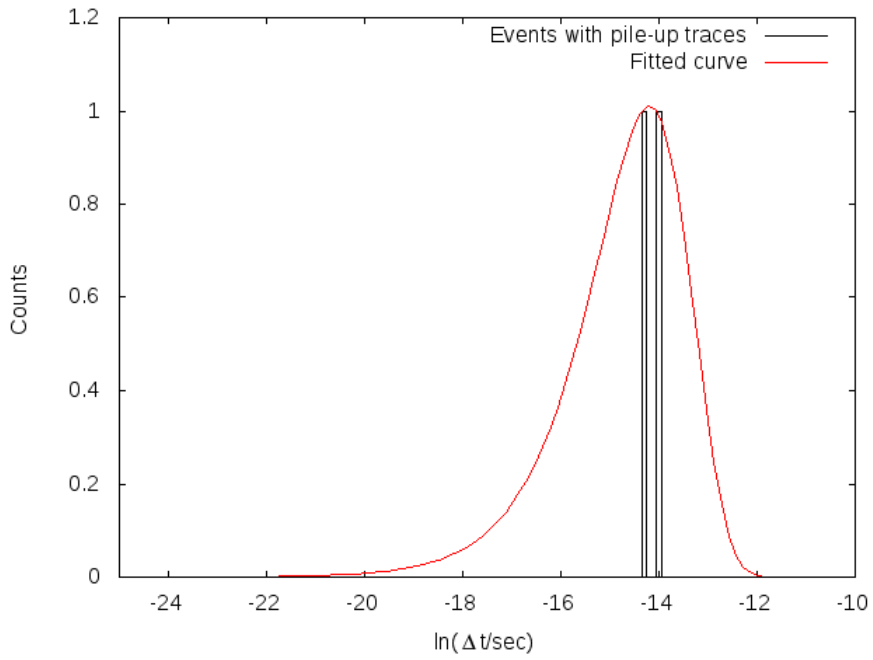

Figure 4.19: Fit made on Δt_2 with Function 4.2.

$\sigma_{\Theta_{exp},min}$=0.04 and upper limit $\sigma_{\Theta_{exp},max}$=1.83 for two events, with the expectation value for $\sigma_{\Theta_{exp}}$ being 0.69. Though being weak, it might be a suggestion that the two events originated from the same species of radioactivity in terms of Δt_2.

A fit (see Figure 4.19) was done with the Function 4.2 with returned λ=9.55×10^5 s^{-1}. Due to the relation $\lambda = ln2/T_{1/2}$, the fitted value for $T_{1/2}$=0.72±0.36 μs, which is close to the already-known $T_{1/2}$=0.62 μs of ^{105}Te.

As with Δt_1, one has to assume that the α-particle emitted by ^{113}Ba existed without being detected. Thus, the distribution of Δt_1 is taken as reflecting the lifetime of the hypothesized ^{113}Ba with standard deviation $\sigma_{\Theta_{exp}}$=0.66 falling between the expected upper and lower limits. It is very close to the expected value 0.69. A similar fit is applied to Δt_1 (see Figure 4.20). The fitted values for λ is 6.682 s^{-1}, corresponding to $T_{1/2}$=0.10±0.05 s and can be considered as the upper limit for the half-life of ^{113}Ba, if both of the pile-up events were due to ^{113}Ba decay.

For comparison, if the first pile-up trace shown in Figure 4.16 is considered as a true double α-decay chain of ^{109}Xe with double-escaping, the half-lives will be calculated as

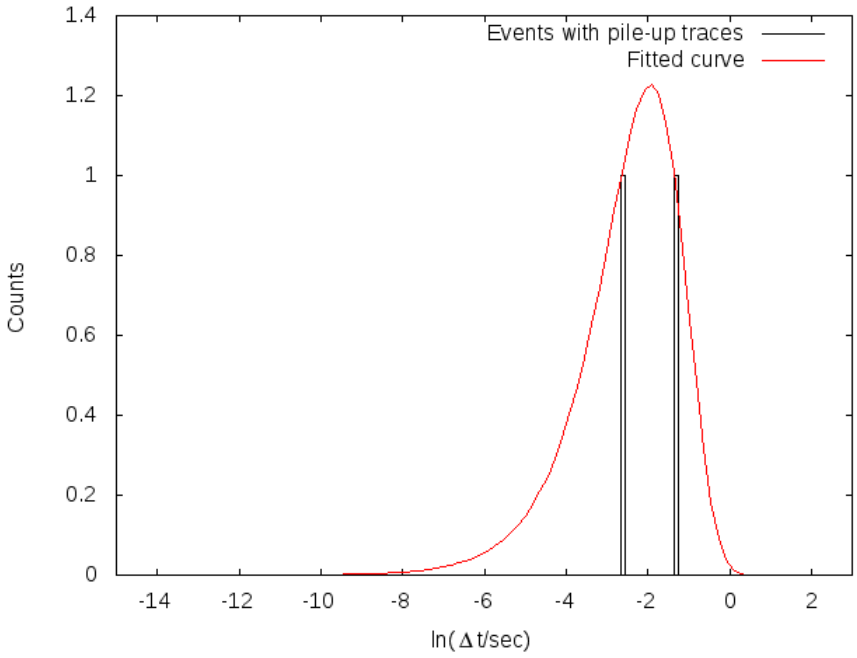

Figure 4.20: Fit made on Δt_1 with Function 4.2.

$T_{1/2}$=0.084±0.046 s for the group of first decay for all three events and $T_{1/2}$=0.37±0.20 μs for the group of second decays (see Figure 4.21 and 4.22). The fitting results shows that the three events originate from the same species of radioactivity. The results do not deviate much from the case where the first pile-up trace is excluded.

Summed signal

The measured height of the output by the energy filter is only valid if the filtered pulse is sufficiently well separated in time from its preceding and succeeding pulses so that their peak amplitudes are not distorted by the action of the trapezoidal filter. Since the trapezoidal filter is linear, the output of it for a group of pulses is the sum of its output for individual pulses in this group. Pile-up occurs when the rising edge of one pulse lies under the peak of its neighbour. In Figure 4.23 [41], the situation for pulse 2 and 3 is the case we have dealt with above where an offline trapezoidal filter resolves the energies. Considering the rise time of the trigger filter as short as 0.1 μs and the flat top of zero, it is possible that the pile-up inspector of Pixie-16 is not able to distinguish two closely spaced pulses if the time interval

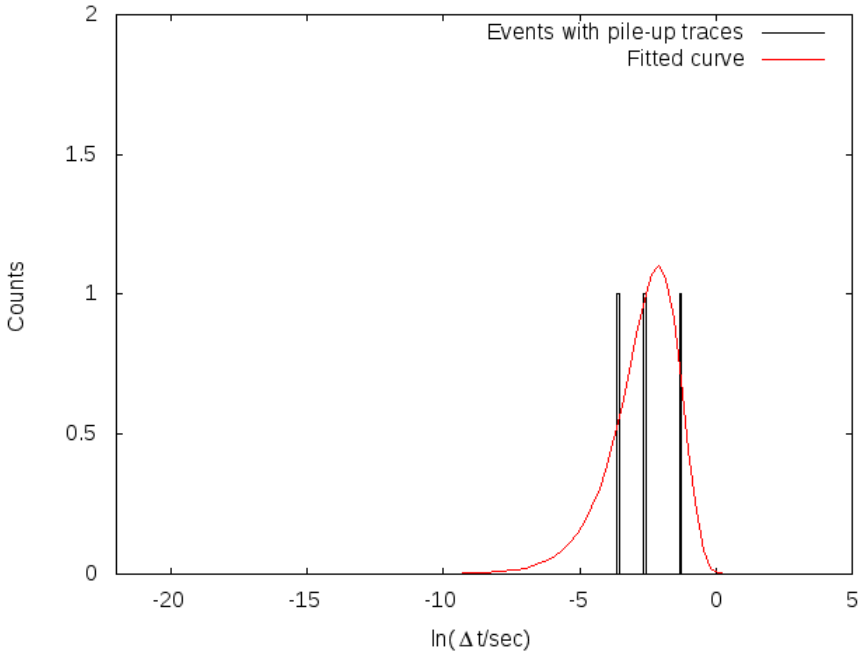

Figure 4.21: Fit made on Δt_1 for all three pile-up traces.

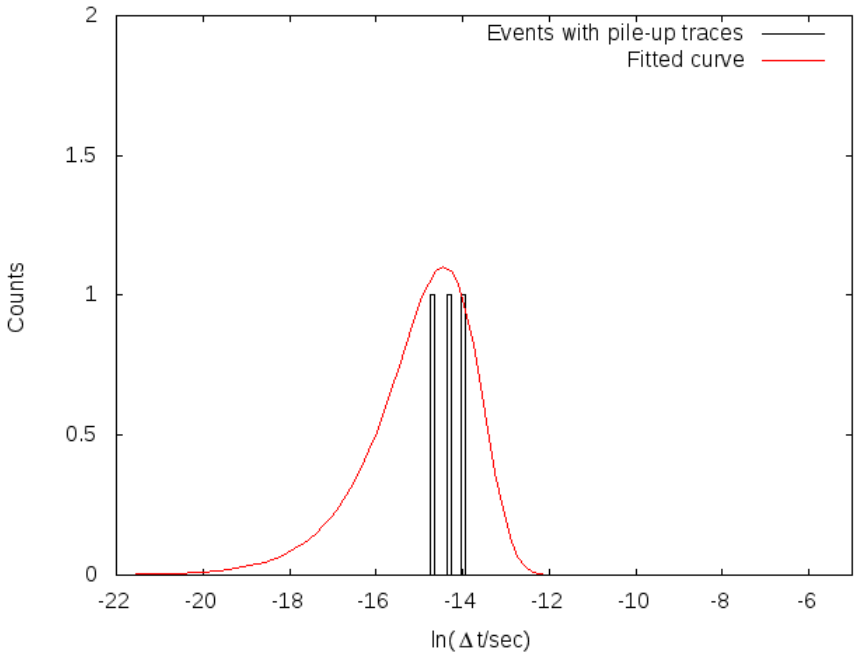

Figure 4.22: Fit made on Δt_2 for all three pile-up traces.

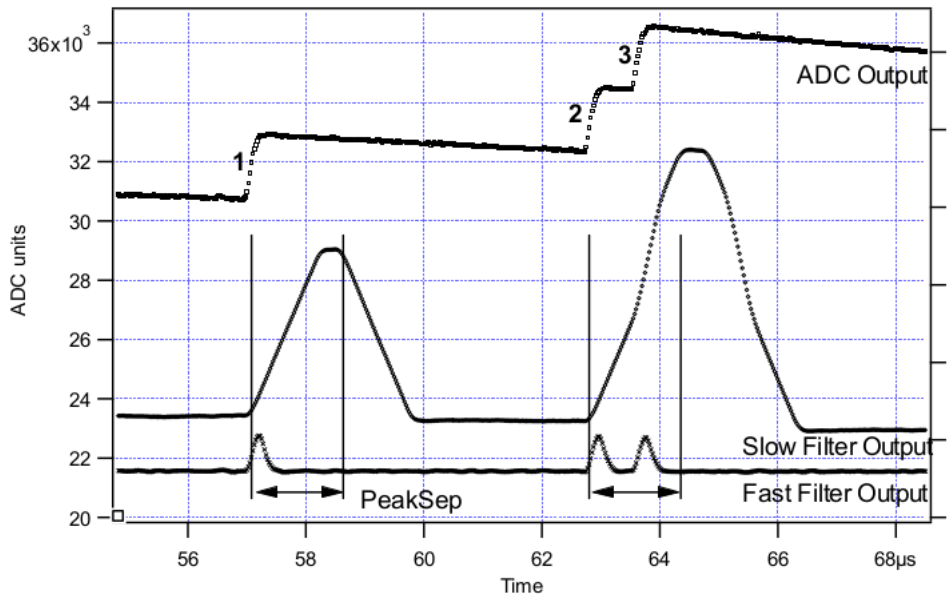

Figure 4.23: Illustration of inspection of pulse pile-ups.

between them comes below to 0.2 μs. The output of the trigger filters for the two pulses will overlap and the pile-up signal will be mistaken as a huge "summed" signal. In our case, the summed signal is the sum of α-particles emitted by ^{109}Xe and ^{105}Te whose energy can be higher than 8 MeV.

Another correlation matrix was set up to look for such summed signal correlated backward to the α-particle emitted by ^{113}Ba. According to the prediction of total half-life $T_{1/2}$=0.08 s, the maximum time window was changed to be 5 s for the time interval between correlated signals, which is more than 50 times as long as the expected half-life. Because of the fine structure of the decay chain ^{109}Xe $\rightarrow$ ^{105}Te $\rightarrow$ ^{101}Sn, the second signal, referred as the summed signal, is expected to fall between 8383 keV and 8942 keV with the worst energy resolution of DSSD of 3.5% considered. The first signal in correlation is expected to fall between 3738 keV and 4011 keV.

As shown in Figure 4.15, the correlation matrix in the upper panel appears to be very noisy, filled with random correlation. In the zone of interest, the statistics seems to be relatively low (see Figure 4.24). Empirically, the energy of β-delayed α-particles/protons from nuclei above ^{100}Sn fall within the range from 2 MeV to 9 MeV which to some extent

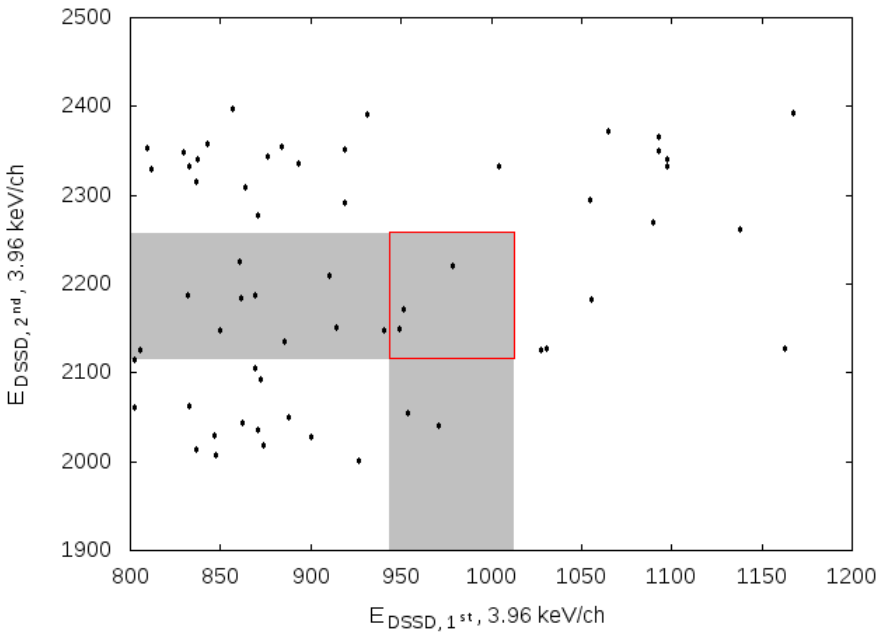

Figure 4.24: Correlation matrix for searching summed α-particles from ^{109}Xe and ^{105}Te in correlation with the α-particle from ^{113}Ba. The time window is 200 ms. Horizontal and vertical shaded bars are expected energy for the first and second signals based on energy resolution of DSSD. The overlapping area is the zone of interest.

overlaps with our zone of interest for the summed signal. Therefore, the anti-coincidence on β-decay signals are required for signals put into the correlation matrix for background reduction.

The time intervals of the three events in the zone of interest are 81.7 ms, 48.7 ms and 28.9 ms respectively. These values are at least two times longer than the half-life of ^{109}Xe. Because they don not form a narrowly correlated cluster in energy-energy plot, only one of them could be a candidate and because of the level of the background, we cannot claim these events as candidates.

4.2.3 Gound-state to Ground-state β-decay Branch

Another signature for ^{113}Ba decay uses its beta-decay, the most prevalent decay mode followed by proton emission of ^{113}Cs which decays via proton emission with $T_{1/2}$=17.7 μs and S_p=-974±3 keV.

Here in order to reconstruct the whole decay process, one has to collect all of the three elements: the ion implantation in a certain pixel, the β-decay signal afterwards and the direct proton emission from the ground-state of ^{113}Cs in the same pixel as the preceding ion. The correlation of decays back to the preceding ion is similar to what was done in the analysis for α-decays. However, the biggest difference lies in correlations of β-decay signals backward in time to ion implantation and forward to proton emissions. The overwhelming background of β-delayed proton emitters makes the count rate very high of either the direct measurement of positron or the related 511 keV photons. Thus, it is difficult to identify the ion-proton chain on DSSD to which an observed β-decay signal should be correlated. A solution to this problem is to make correlation between all β-decay signals and local ion-decay pairs.

Two 40×40 matrix as containers of time intervals were constructed where each element corresponds to a pixel on DSSD. The reconstruction of the decay process starts with identifying an ion. Whenever a β-decay signal is observed later on, the time difference of it with respect to a already-existed ion Δt_1 will be calculated and saved in the corresponding element in the first matrix. Then a correlation between a proton and an ion in the same pixel is made, with the time difference Δt_2 between the β-decay signal and this proton saved in the corresponding element in the second matrix (see Figure 4.25). After the correlation is completed, the β-decay signal will be kept while for this pixel the record of ion as well as the proton will be removed until the next ion comes in.

This method provides a good way to recover the real β-decay in correlation to the proton-emission, though, a lot of false correlation are present due to the fact that the β-decay signal can only be related to one ion and one proton at a time. The proton emitter, ^{113}Cs, as one of the most abundant contaminants directly produced in reaction, contributes to background of protons too. This ambiguity can be eliminated by limiting the time difference between the proton and the ion greater than 177 μs which is ten times greater than the half-life of ^{113}Cs.

Because of the fact that the component of positrons is not complete in the front Si-PIN and overwhelmed by β-delayed protons in both veto detectors, the only signal that can be

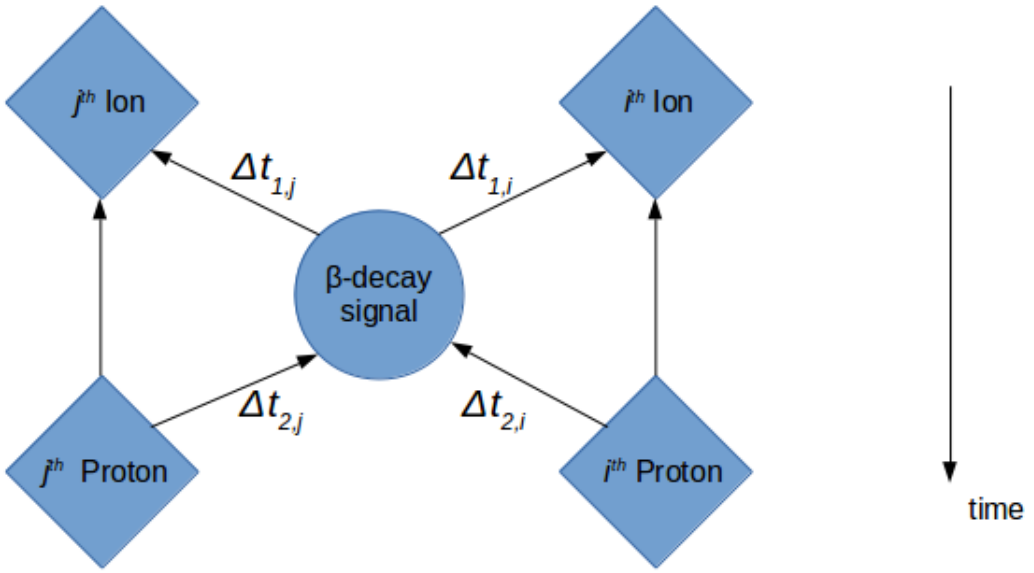

Figure 4.25: Illustration of procedures of reconstructing ground-state to ground-state β-decay of ^{113}Ba in correlation to proton-emission of the β-decay daughter ^{113}Cs. The arrows indicate the direction of correlation. Δt_1 and Δt_2 are saved in the corresponding element in the two time matrix.

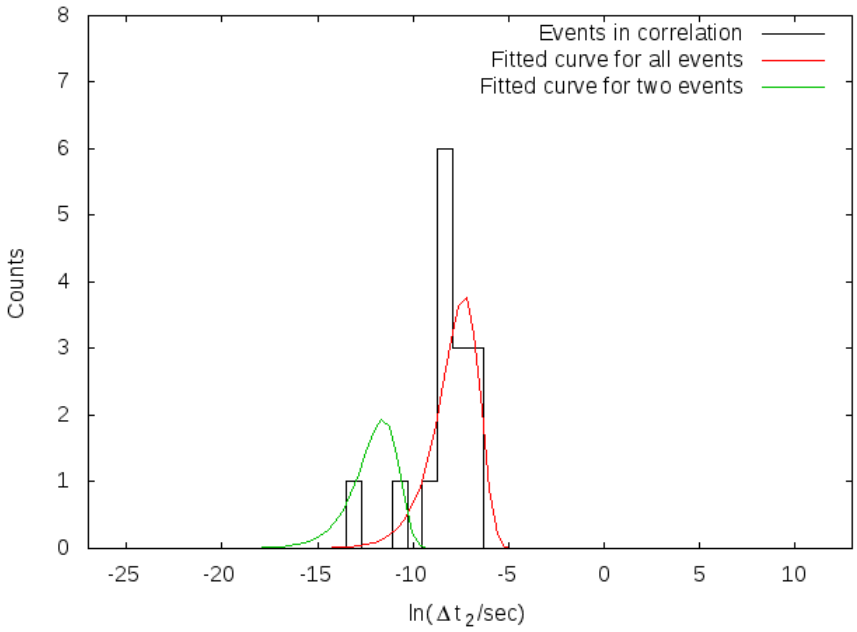

Figure 4.26: Distribution of Δt_2 of decays in correlation with β-decay and local ions with primary beam energy at 245 MeV.

related to β-decays is the 511 keV photons generated from electron-positron annihilation, though it only visible to the plug-in part of the NaI detector array.

For the primary beam at 245 MeV, the distribution of Δt_2 is shown in Figure 4.26, where all values for Δt_2 are put into logarithmic time scale. 15 decay events were observed as shown, satisfying the above conditions. A fit with Function 4.2. The returned value from fit for the decay constant λ is 1359 s^{-1} which gives half-life $T_{1/2}$ of 509$\pm$158 μs. This does not match the known half-life of ^{113}Cs of 17.7 μs and is indicative of random correlations. However, the two counts on the very left side seem to be far away from the other counts with Δt_2 being 17.36 and 3.03 μs respectively.

A second fit with the same form of function was made on these counts, returning $T_{1/2}$=5.64 $\pm$3.27 μs. The standard deviation of the distribution of these two events was 0.87, falling in the reasonable range above 0.04 and below 1.83, close to the expected value σ_Θ=0.69. This suggests that these two events might arise from the same species

of radioactivity and that they are good candidates for proton-emissions from ^{113}Cs following ground-state to ground-state β-decay of ^{113}Ba.

It is then necessary to estimate the error probabilities for the correlated events, which is in fact the probability, P_{err}, that a fluctuation of the background distribution produces the observed number of correlations or more in the interval from a certain time point (t_{min}) to infinity. As proposed in Reference [43], it is equal to the sum over Poisson's distribution:

$$P_{err} \approx \Sigma_{n=n_m}^{\infty} \frac{n_b^n}{n!} e^{-n_b} \tag{4.5}$$

where n_b is the expected value for the number of observed correlations, n is the number of correlated events observed. The procedure has to be repeated individually for each pixel where correlated events appeared. For the count on the right side under the green curve in Figure 4.26 with Δt_2=17.36 μs, the P_{err} is calculated to be 0.82 while for the other counts on the left next to it with Δt_2=3.03 μs, the P_{err} is calculated to be 0.68. Thus, one can draw a conclusion that it is highly possible that these two events are produced by stochastic fluctuation of background instead of being real candidate for the ground-state to ground-state β-decay of ^{113}Ba followed by direct proton emission of ^{113}Cs.

For the data with primary beam at 250 MeV, the statistics of ^{113}Cs protons in correlation is more than that with lower beam energy. After repeating the fit on this data group (see Figure 4.27), the returned λ is 2505 sec^{-1} which corresponds to $T_{1/2}$=276 μs. Thus, there is no candidate for ground-state to ground-state β-decay of ^{113}Ba with higher beam energy.

4.2.4 β-delayed Proton Emission

In the β-delayed proton emission, the mother nucleus emits a positron and thus decays to excited states in the intermediate nucleus. Shortly afterwards, a proton is emitted and thus the whole process is completed.

In the vicinity of ^{113}Ba, the change in S_p and Q_{EC} is smooth thus its neighbours exhibit wide-spreading spectrum of β-delayed protons which overlap with each other to a large extent. It is difficult to recognize β-delayed protons solely depending on their energies. A

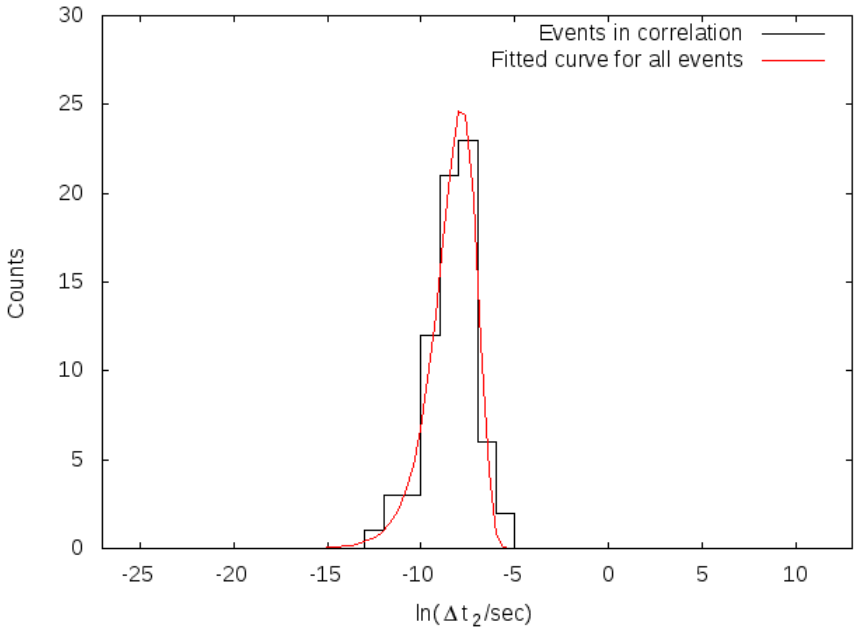

Figure 4.27: Fit on data with beam at 250 MeV.

more accessible way is to analyse the time distribution of delayed protons with respective to the preceding ion, the implantation of mother nuclei.

The reconstruction of this decay process requires a preceding ion implantation in a certain pixel and a subsequent decay signal with possible energy from 1.5 MeV to 9 MeV based on extrapolation from that of its neighbouring nuclei. The decay signal is required to be in coincidence with 511 keV photons registered in the plug-in part of the NaI detector array. Once the correlation between the decay and the ion is made, the needed information will be deduced and saved and the correlation has to be reset.

The energy distribution of decay signals in correlation is shown in Figure 4.28. The energy spectrum of decays in coincidence with β-decays (511 keV photons) is almost indistinguishable with the βp spectra of neighbouring nuclei like ^{113}Xe, peaking at 3 MeV, except that escaping protons deposited energy below 2 MeV. This is a good sign that regardless of the total efficiency for the observation of β-decays, this method provides a relatively clean signature of β-delayed protons.

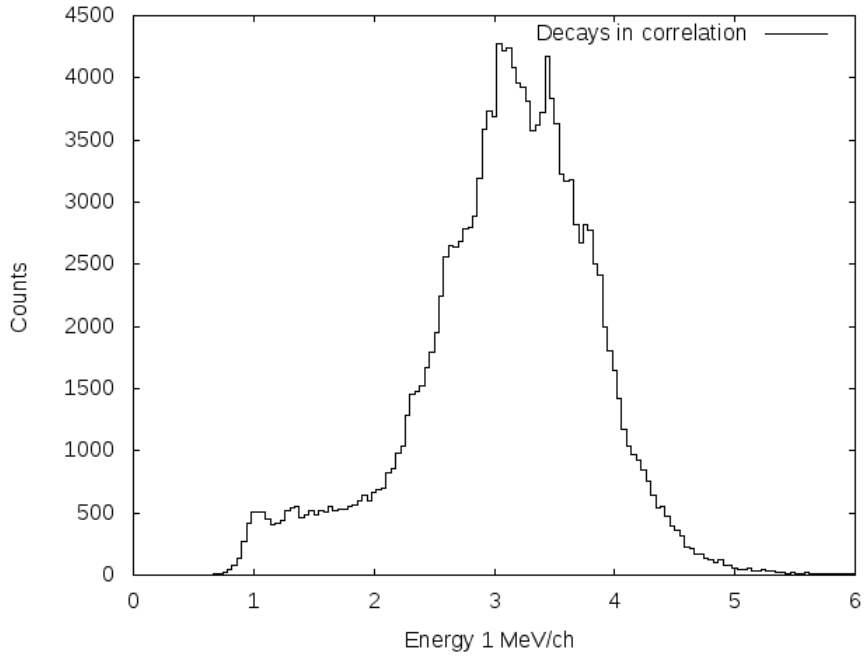

Figure 4.28: Distribution of protons in coincidence with 511 keV γ-rays, correlated to preceding ions in the same pixels

As above, the time difference between the decay and the local ion Δt is plotted in logarithmic time scale. In total, there are 170876 counts in collection as seen in Figure 4.29. Unfortunately, no fine structure suggesting different species of radioactivity is present in the distribution. Thus, it is impossible to tell the β-delayed protons from ^{113}Ba from the overwhelming background.

4.2.5 β-delayed α-particle Emission

In search for the β-delayed α-emission branch of ^{113}Ba, the goal is to reconstruct the full decay chain $^{113}\text{Ba} \rightarrow {}^{113}\text{Cs} \rightarrow {}^{109}\text{I} \rightarrow {}^{108}\text{Te}$. One has to observe a β-delayed α-particle at energy of several MeV above the Q_α=3.487 MeV of ^{113}Cs and then the proton emitted from the ground-state of ^{109}I at the energy of 812 keV. This requires correlations involving a preceding ion implantation and two generations of decay signals separated by the time difference Δt whose distribution agrees with $T_{1/2}$=93.5 μs of ^{109}I.

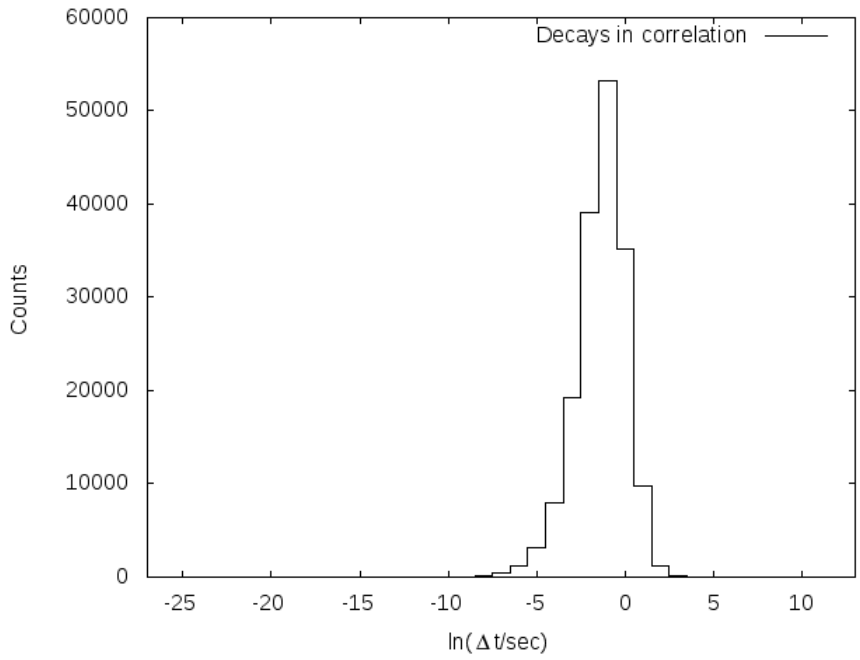

Figure 4.29: Energy distribution of protons correlated to preceding ions in the samel pixel in coincidence with 511 keV γ-rays.

The maximum time window allowed for the correlations between two generation of decays is set to 2 ms which is more than ten times longer than the half-life of ^{109}Te and thus a large fraction of backgrounds can be eliminated. As long as the decay chain is completed or the second decay comes beyond this time window with respect to the first decay signal, the whole chain will be reset. With the consideration of the poor efficiency with the plug-in part of the NaI detector array for 511 keV, no additional coincidence or anti-coincidence is applied on decay signals.

A pair of correlated signals was found in this search (see Figure 4.30). The energy of the first signal is 7557 keV while the energy of the second one is 772 keV. The two signals are separated by 65.8 μs and the preceding ion is 0.339 s prior to the leading decay. No 511 keV γ-ray came with either decay.

Generally, 7557 keV is reasonable for a β-delayed α-particle while 772 keV is considered a bit lower than the energy of proton emitted by ^{109}I at 812 keV. However, some explanation

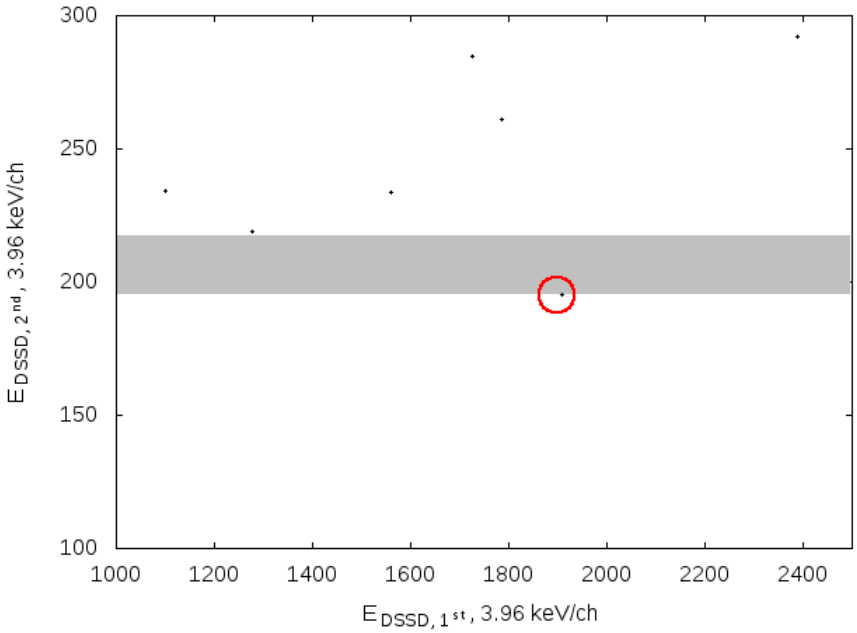

Figure 4.30: Correlation matrix for potential β-delayed α-particles of ^{113}Ba correlated to subsequent proton emitted by ^{109}I. The event in the red circle is the most probable event with reasonable energy for both decays. The shaded area is the expected energy range for proton-emission of ^{109}I.

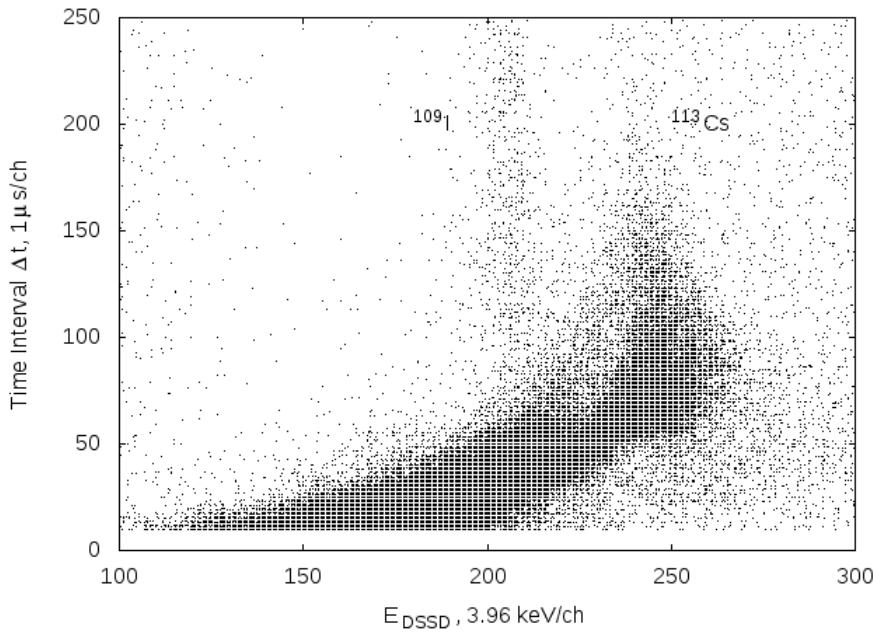

Figure 4.31: Energy of decays (x-axis) versus time interval (y-axis) between decay and preceding ion-implantation. The "golf-club" shape is present.

may be given by the time interval Δt=65.8 μs between these pulses that the lower-than-expected energy might be due to the response of the on-board trapezoidal filter to a smaller signal closely following a large signal in time. In this case, the second signal is superimposed on the exponentially decreasing tail of the first one, which results in a decreasing baseline needed for determination of the energy of the second pulse. In the energy versus time spectrum where the time refers to the time interval between the ion-implantation and the subsequent decay, this feature is present as the so-called "golf-club" shape (see Figure 4.31). The closer the Δt is, the smaller energy of the second pulse is deduced.

From gaussian fit on the proton peak of ^{109}I, the full width at half maximum (FWHM) of the peak is 42.4 keV with the centroid of the peak at 812 keV. In the comparison of the second signal in this correlated pair with proton peaks of ^{109}I, it is found that the energy of this signal is at the left margin of the proton peak of ^{109}I (see Figure 4.32). Thus, it is necessary to figure out whether it is simply the underestimation due to the "golf-club" effect or not. A simulation on the response of the on-board digital trapezoidal filter to this

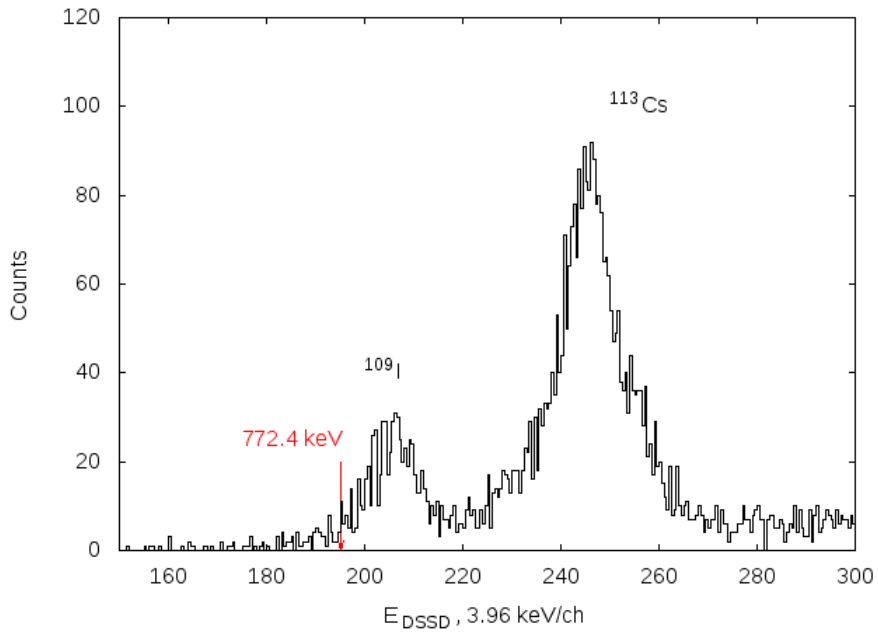

Figure 4.32: Energy of the potential candidate of proton from ^{109}I (pointed out by the red arrow) in comparison with proton peak of ^{109}I. The energy distribution of decay signals is a projection of Figure 4.31 onto x-axis, with time difference Δt larger than 50 μs.

particular case is made for quantifying the dependence of the energy of the second signal on the time interval in between.

In the first step, a fit on the wave form output by the preamplifier gives the decay constant of 29 μs. Then two exponentially decaying pulses are generated by C++ code in step of 10 ns which agrees with the sampling period of analog-to-digital (ADC) of Pixie-16 module. The amplitude of the two pulses are set to 7557 keV and 772 keV as observed. The time interval of the two pulses is set to 65.8 μs.

In the second step, an algorithm which simulates the on-board algorithm [50] implemented by XIA into Pixie-16 module is created for reproducing the energies of pile-up signals with C++ language. It reads in the simulated digital signals generated above. The algorithm incorporates a trigger filter and energy filter. As mentioned before, the rise time and the gap time of the trigger filter are 0.1 μs and 0 μs respectively. The rise time and gap of the energy filter are 6 μs and 1.2 μs respectively. A constant τ in this algorithm was set to 35 μs in order to compensate the descending tail of the first pulse on which the second one rides.

All these parameters were tested, adjusted and finally determined so that the result is in constancy with the observation in experiment.

The deduced energy of the second pulse from the simulation is 778 keV, with 0.7 % error compared to the measured value 772 keV. The difference is well within the energy resolution of DSSD of 5.2 % near 812 keV. The simulation suggests that there is possibility that the only pair of correlated decays is a candidate of the potential β-delayed α-particle emission branch.

Again, it is straightforward to use the same method to estimate the error probability of this correlated events. The probability P_{err} that this event is produced by stochastic fluctuation of background is calculated to be on the order of 10^{-7}. which indicates that this is a good candidate for the $\beta\alpha$-emission branch of ^{113}Ba.

Chapter 5

Disscussion

5.1 α-decay of ^{113}Ba

Since no evidence of decays of ^{113}Ba was discovered when the energy of the primary beam was set to 250 MeV, all conclusions drawn below are based on $E = 245$ MeV data. In order to estimate the overall half-life of ^{113}Ba, we have to evaluate the time difference between the preceding local ions and the subsequent events. The time difference between the two α-decay pile-up traces and the the respective preceding ion implantations are 270 ms and 72 ms. If the already-known lifetime for α-decay of ^{109}Xe τ=18.7 ms is subtracted from these two values, the maximum allowed time for α-decay in this case are 251.3 ms and 53.3 ms respectively. For the candidate of the β-delayed α-emission branch, the corresponding time difference is 399 ms. Thus, by averaging over these values and taking uncertainties of measurement into consideration, we have the measured lifetime of ^{113}Ba: τ=222$\pm$141 ms.

As for the partial half-life of α-decay branch, it can be evaluated theoretically by using the phenomenological formula (see Expression 5.1) for α-decay half-lives [51]. This formula starts with the classical Gamow picture of α-decay including the formation, collision and penetration an α-particle. The penetration probability was evaluated by Taylor's expansion and integrated analytically. Free parameters were fitted from experimental ground-state $0^+$to ground-state 0^+ for even-even nuclei. The phenomenological formula was taken up to

forth order term based on the convergence of parameters. The formula gives a consistent prediction of the partial half-life of s-wave α-decay for heavy and super-heavy ions beyond trans-lead regions.

$$\begin{aligned} log_{10}T_\alpha(s) = & 1.7195\sqrt{\frac{A-4}{A}}Z_D/\sqrt{Q_\alpha(MeV)} \\ & - 1.2901\sqrt{\frac{A-4}{A}}\sqrt{RZ_D} \\ & + 0.07466\sqrt{\frac{A-4}{A}}R^{3/2}/Z_D^{1/2}\cdot Q_\alpha(MeV) \\ & + 0.005499\sqrt{\frac{A-4}{A}}R^{5/2}/Z_D^{3/2}\cdot (Q_\alpha(MeV))^{3/2} \\ & - log_{10}N - 0.159175 + h \end{aligned} \tag{5.1}$$

By taking the calculated Q_α=4.02 MeV by finite range droplet model (FRDM) for ^{113}Ba [33] into account, we have the calculated $T_{\alpha,1/2}$=1.79 s. This result is not consistent with $T_{1/2,\alpha}$=0.54 s obtained by density-dependent cluster model (DDCM) calculation [33]. Obviously, the calculated result with this formula is so sensitive to small changes in Q_α input that an increase of 0.1 MeV will lead to much shorter $T_{1/2,\alpha}$=0.521 s. However, it is argued [32, 33] that predicted values for Q_α of Cs and Ba isotopes by FRDM agree well with experimental values. It is then necessary to see if this formula is able to reproduce half-lives of some already-known α-emitters in this region.

Another option is to make prediction with the universal decay law (UDL) for α-decay [52]. This method is derived from the microscopic description of α-decay and cluster emission based on R-matrix theory. The expression can be generalized in the form:

$$log(T_{1/2}) = a\chi' + b\rho' + c \tag{5.2}$$

where free parameters a, b, c are fitted from 139 α-decay events from emitters with 78$\leq$ Z $\leq$108. The $T_{1/2}$=6.35 s predicted by this method is more than one order of magnitude longer than that by DDCM.

Shown in Table 5.1 is the comparison among the values for half-lives obtained from experiments, calculated by DDCM, phenomenological formula and the UDL formula. It is clear that the DDCM gives the best agreement with experimental values while results by phenomenological formula are generally one order larger and the results by UDL are even worse.

The reason for the discrepancy by phenomenological formula lies in the fact that experimental data upon which the free parameters are fitted use heavy nuclei. These values contain information on formation probability of α-particles in that heavy mass region instead of the much lighter and more symmetric ^{100}Sn region. Specifically, the term $log_{10}N = log_{10}N_{coll} + log_{10}P_{form}$ in Formula 5.1 includes the formation probability of the alpha-particle inside the mother nucleus. Considering the $log_{10}N_{coll}$ almost remains the same for these two mass region, this is a hint for larger formation probability of α-particles since if larger P_{form} were expected for α-emitters in ^{100}Sn region, shorter half-lives would be obtained.

For UDL formula, this problem is similar that no sufficient data were provided from ^{100}Sn region for fitting of free parameters. The deeper reason is related with the estimation on formation probability of α-particles. The parameter c in Formula 5.2 is expressed as:

$$log(\frac{cot\beta ln2}{\nu R^2 |F_c(R)|^2}) \tag{5.3}$$

where the formation probability $F_c(R)$ dominants. Similarly, small increase in $F_c(R)$ compared to that of heavy nuclei can lead to great decrease in calculated half-life.

5.2 β-decay Branch

Up to now, we have been relying on the prediction by Reference [38] that $T_{1/2,\beta}$=100 ms. This is a result obtained from quasi-particle random phase approximation (QRPA) method. If this was reliable, the predicted overall half-life of ^{113}Ba is calculated to be 0.084 s which lies within the error bar of the measured upper limit given above. In addition, a shell model calculation

Table 5.1: Comparison among experimental partial half-life of some α-decaying nuclei above ^{100}Sn, theoretical calculations using DDCM (column 4), phenomenological formula (column 5) and UDL formula (column 6).

Nucleus	Q_α(MeV)	$T_{\alpha,Exp}$(Exp)(s)	$T_{\alpha,Cal1}$(s)	$T_{\alpha,Cal2}$(s)	$T_{\alpha,Cal3}$(s)
^{105}Te	4.900	7.0×10^{-7}	5.4×10^{-7}	1.7×10^{-6}	6.4×10^{-6}
^{106}Te	4.290	7.0×10^{-5}	1.1×10^{-4}	1.5×10^{-4}	2×10^{-3}
^{107}Te	4.008	4.4×10^{-3}	3.8×10^{-3}	1.1×10^{-2}	4.3×10^{-2}
^{108}Te	3.445	4.3	3.9	0.688	62.16
^{109}Te	3.23	1.2×10^{2}	1.7×10^{2}	441.995	1580.48
^{110}Te	2.723	2.8×10^{6}	1.3×10^{6}	1.5×10^{6}	1.6×10^{7}
^{108}I	4.034	1.0×10^{-2}	1.9×10^{-2}	0.104	0.12
^{110}I	3.58	3.8	6.1	33.17	35.43
^{111}I	3.27	2.8×10^{2}	3.6×10^{2}	1.0×10^{3}	3.5×10^{3}
^{112}I	2.99	2.9×10^{5}	8.7×10^{4}	4.4×10^{5}	4.2×10^{5}
^{113}I	2.705	2×10^{7}	1.5×10^{7}	3.9×10^{7}	1.14×10^{8}
^{109}Xe	5.067	1.3×10^{-2}	2.9×10^{-2}	7.7×10^{-2}	2.9×10^{-1}
^{110}Xe	3.885	1.1×10^{-1}	1.5×10^{-1}	0.2	2.56
^{111}Xe	3.693	2.5	2.6	8.4	30.2
^{112}Xe	3.33	3.4×10^{2}	3.7×10^{2}	5.2×10^{2}	6.1×10^{3}
^{113}Xe	3.094	7.8×10^{3}	3.3×10^{4}	9.7×10^{4}	3.1×10^{5}
^{114}Cs	3.357	3.2×10^{3}	2.9×10^{3}	1.7×10^{4}	1.7×10^{4}
^{114}Ba	3.540	48	260	389	4.4×10^{3}

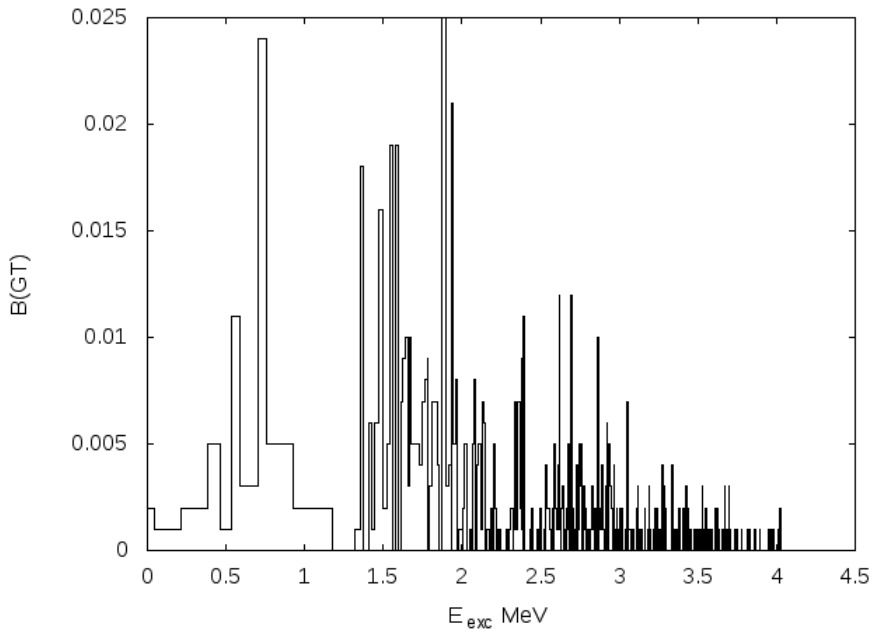

Figure 5.1: Reduced transition matrix elements $B(GT)$ by shell model calculation.

was made using NushellX code [53] and sn100pn interaction used previously in Reference [21]. The input $Q_{\beta+}$=13.824 MeV was obtained from liquid drop model calculation. The reduced matrix elements $B(GT)$ for Gamow-Teller transitions were obtained for excitation energy up to 4.08 MeV (see Figure 5.1). The energy cutoff was made mainly due to the fact that the overwhelmingly large amount configuration in ^{113}Ba from single particle proton and neutron states $g7/2, d5/2, s1/2$ and $h11/2$ which were used. This exceeded the capabilities of the code and computer. The distribution of $B(GT)$ lead to the predicted $T_{1/2,\beta}$=0.0297 s which is shorter than the QRPA results. However, including the conventional quenching factor which is due to the shell model truncation, one can obtain $T_{1/2}$ in the range of 100 ms. Besides both calculation with physical model, an estimation on β-decay partial half-life can also be obtained from extrapolation from systematics of $log(ft)$ values of already-known odd-A barium isotopes ^{115,117,119}Ba. The $Q_{\beta+}$ input into calculation of Fermi integral is extrapolated from that of neighbouring barium isotopes as well (see Figure 5.2, additional 1.1 MeV should be subtracted from these values for β-decay). Shown in Figure 5.3 is the extrapolation of $log(ft)$ for ^{113}Ba. In this way, the $T_{1/2,\beta}$ of it is determined to be 0.165

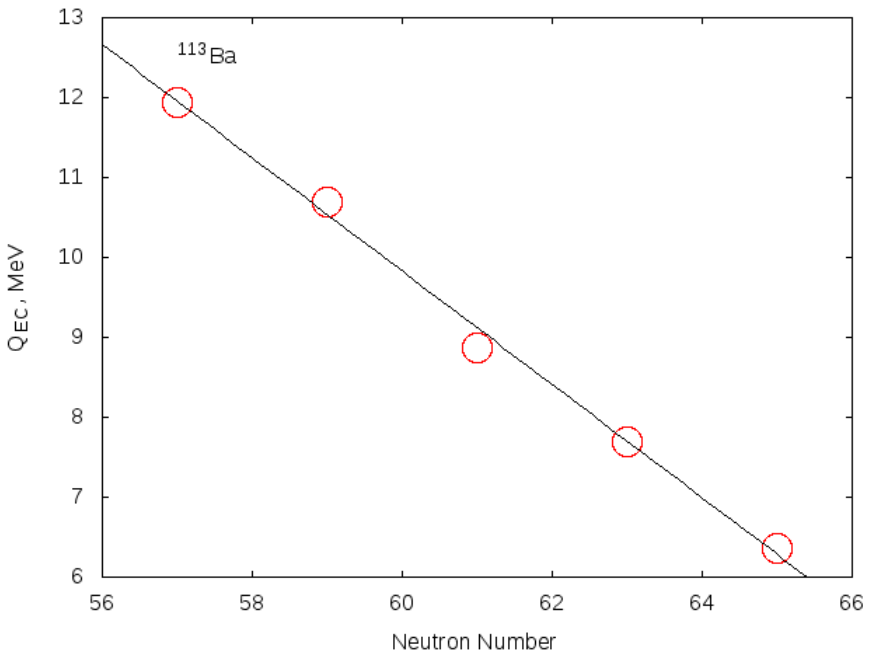

Figure 5.2: The Q_{EC} of ^{113}Ba is extrapolated from odd-A barium isotopes up to N=65.

s which is more compatible with QRPA calculation. As mentioned before, the relatively smooth Q_{EC} in this region suggests similar behaviour of β-decay.

Depending on the predicted half-life $T_{1/2,\alpha}$=0.54 s and $T_{1/2,\beta}$=0.1 s, the branching ratio for β-decay is 84.4 % thus α-decay b_α is 15.6 %. The overall half-life $T_{1/2}$ is predicted to be 0.084 s which lies within the error bars of the measured upper limit given above. This also implies that similar to that of the neighbouring barium isotopes, the dominant decay mode of ^{113}Ba is β-decay.

As mentioned before, the shallow implantation depth of the incoming ions makes it easy for the internally emitted α-particle to escape from the front side of DSSD, where the probability of full energy deposition ranges from 51$\sim$54 % for α-decays of ^{113}Ba, ^{109}Xe and ^{105}Te. Based on these values, if the two candidates for the pile-up traces are believed to be real and follow the "missing" α-particle emitted by ^{113}Ba, the upper limit for the probability that one only sees the complete pile-up traces without seeing the preceding α-particle is estimated to be in the range from 12.8 % to 12.9 %. In other words, if the detection probability for full energy deposition of α-particles were 100 %, at least 15 α-decay events

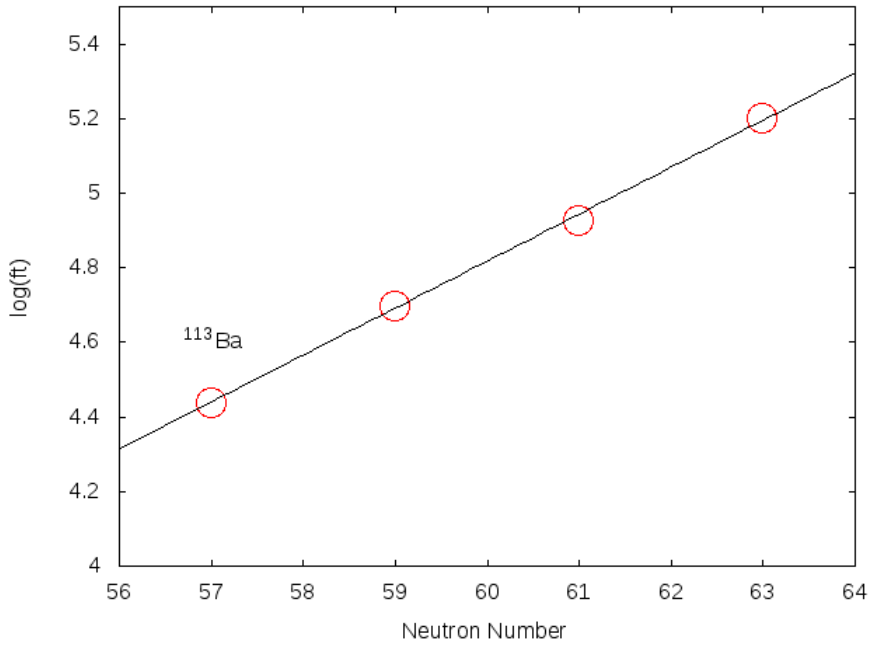

Figure 5.3: Extrapolated $log(ft)$ value of ^{113}Ba from neighbouring odd-A barium isotopes.

of ^{113}Ba could have been observed at the focal plane of the RMS. By taking 15 events into calculation for production cross section for ^{113}Ba with the transmission efficiency of the RMS around 5 %, the production cross section σ=6.0±4.6 nb. This value is proposed to be the lower limit of the production cross section.

5.3 β-delayed Charged Particle Emission

Despite the fact that β-delayed proton-emission could not be cleanly observed in this experiment, it is interesting to see what is predicted for this presumed prevalent decay mode of ^{113}Ba. The calculation is made by the β-delayed charged particle emission code DELPA [54].

For the ground state of ^{113}Ba, the unpaired neutron occupies on the $g_{7/2}$ orbital. The initial spin and parity is assumed to be $\frac{7}{2}^+$. For both βp and $\beta\alpha$ emission branch, only ground states 0^+ of ^{112}Xe and $\frac{1}{2}^+$ of ^{109}I are considered as final states. Other parameters input are S_p=-0.974 MeV Q_α=3.484 MeV of the intermediate nucleus ^{113}Cs. The Q_{EC} input

is 12 MeV as above. The energy spectrum of β-delayed protons is given up to 4.8 MeV while the β-delayed α-particle energy spectrum is given up to 7.00 MeV. Both spectra were calculated with a step length of 0.25 MeV.

Among the excited states of ^{113}Cs, the competition occurs mainly between proton emission and γ-ray emission. From 1.3 MeV to 7.4 MeV, the dominant decay mode is proton emission whereas outside this energy range, de-excitation with γ-ray emission dominates (see Figure 5.4). This is a sign that in most cases, β-decay of ^{113}Ba is accompanied with prompt proton emission. The energy range for these delayed protons covers from 2 MeV to 5 MeV with the maximum intensity placed between 2 MeV and 3 MeV (see Figure 5.5). The distribution overlaps with that of its neighbouring β-delayed proton emitters like ^{113}Xe and this explains the difficulty to tell the delayed protons of ^{113}Ba from the overwhelming background. According to DELPA calculation, the branching ratio for β-delayed α-particle emission is extremely small. It is shown in the Figure 5.6 that the relative intensity for delayed α-particle emissions with respect to that of delayed proton emission is as small as 0.23×10^{-6}. The energy distribution ranges from slightly above 5 MeV to below 7.5 MeV with a peaking below 7 MeV. Unfortunately the only candidate of this branch at the energy of 7557 keV falls slightly above the calculated range which is due to the lack of calculated $B(GT)$ values from the shell model beyond 4.08 MeV . However, the β-delayed α-emission is expected to exist and 7557 keV might be a reasonable value for the energy. Also, this might be suggesting that in reality, there is a shift of $B(GT)$ toward higher excitation energy. If this were the case, the branching ratio $b_{\beta\alpha}$ would be higher than expected and thus the energy of the only candidate will fall within the energy range for β-delayed α-particles. This avenue need to be explored by a large scale.

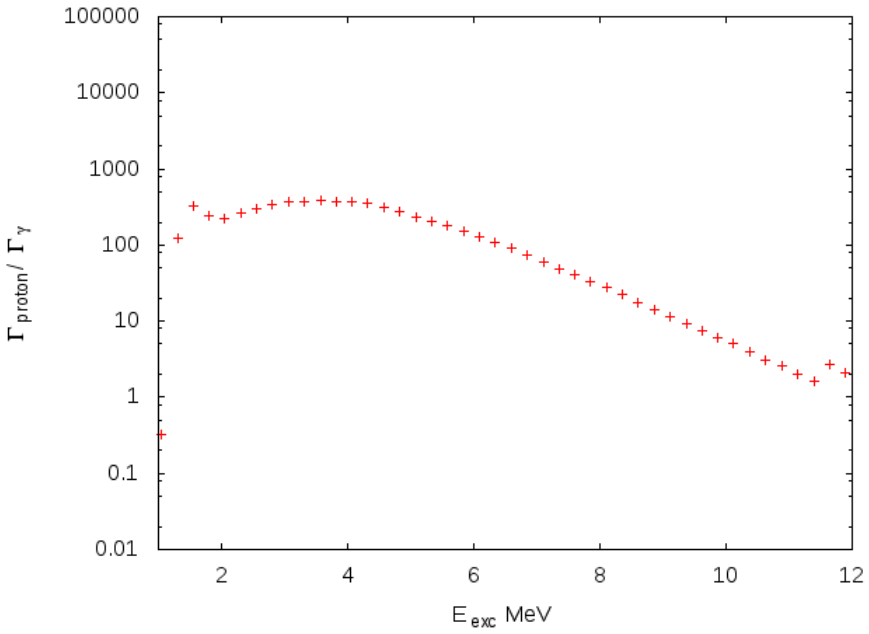

Figure 5.4: Ratio of decay width of proton emission to that of γ-ray emission in terms of excitation energy in ^{113}Cs.

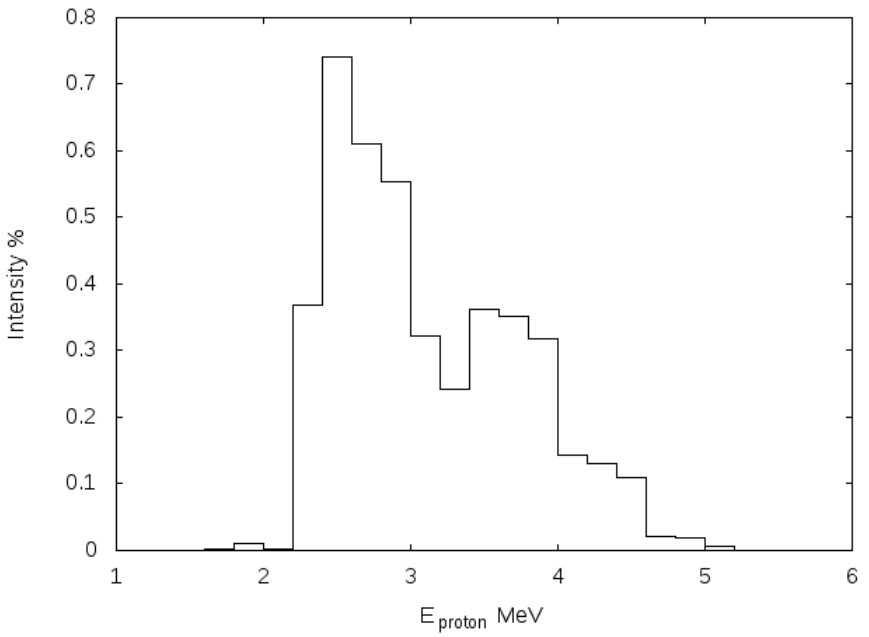

Figure 5.5: Energy distribution of β-delayed protons from ^{113}Ba calculated by DELPA.

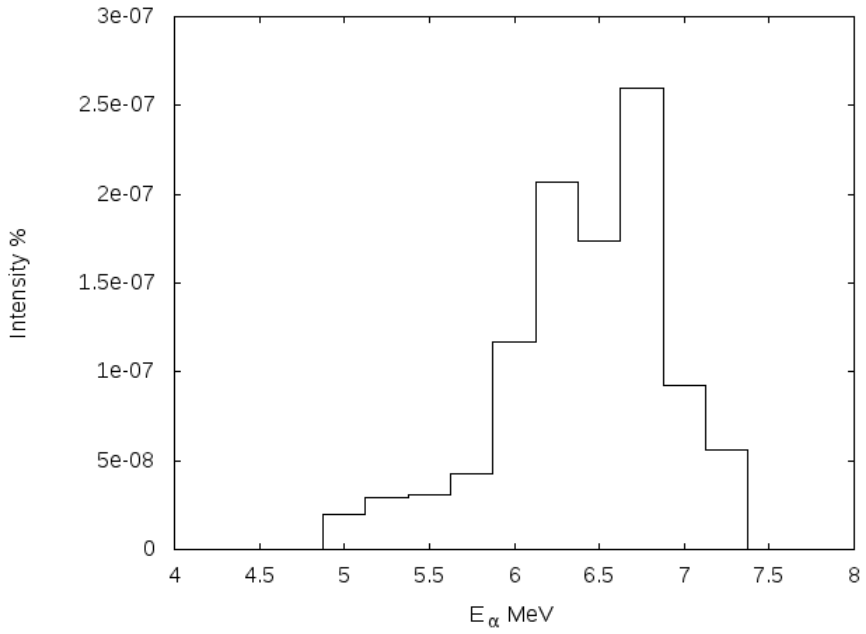

Figure 5.6: Energy distribution of β-delayed α-particle emission of ^{113}Ba calculated by DELPA.

Chapter 6

Summary

This work is aimed at the discovery of one of the heaviest N∼Z nuclei ^{113}Ba via measurement of its four possible decay paths. The α-decay branch, which is the most selective signature of ^{113}Ba, is observed indirectly by recording two pile-up traces ^{109}Xe $\rightarrow$ ^{105}Te $\rightarrow$ ^{101}Sn. The direct α-particles emitted prior to the pile-up traces were not observed possibly due to the too shallow implantation depth of the preceding ^{113}Ba ion and hence α-particles escaped from the DSSD without being detected. Calculations for the partial half-life of α-decay branch were made with several models for ^{113}Ba as well as α-emitters in ^{100}Sn region with known half-lives and we noticed that the lifetimes are often overestimated. This could be a hint for increased α-particle formation probability in this region compared to that of trans-lead region. DDCM shows its reliability in making predictions on half-lives in this region. No solid estimate can be drawn for the reduced α-decay width of ^{113}Ba from the experimental data, but we can provide an upper limit for the overall lifetime τ=222$\pm$141 ms of ^{113}Ba. Consequently, the upper limit of the branching ratio of α-decay and the lower limit of production cross section of 6.0$\pm$4.6 nb of this isotope are obtained. Based on prediction of partial half-life $T_{1/2,\beta}$=0.1 seconds, the branching ratio of α-decay b_α is calculated to be 15.6 %. This is an indication that β-decay is the dominant decay path for this isotope. No reliable candidate was observed for either the ground state to ground state β-decay. The β-delayed proton emission events

cannot cleanly assigned to ^{113}Ba. A candidate for the β-delayed α-particle emission was observed.

On the theoretical side, the reduced β-decay matrix element $B(GT)$ was calculated by nuclear shell model calculation code NuShellX up to the excitation energy of 4.1 MeV. Then the energy spectra of β-delayed proton and α-particle emission of ^{113}Ba were calculated by the code DELPA. β-delayed proton emissions are predicted to be the dominant decay mode in a wide range of excitation energy whereas $\beta\alpha$ branch is predicted to have extremely small decay branch within limited range of energy.

The lesson we learnt from this experiment is that if the barrel part of the NaI detection array had worked with a much lower energy threshold so that 511 keV γ-rays can be detected, the efficiency on identifying β-decay signals would have been improved, compared to 12.5 % currently. Consequently, the number of random correlations for observation of ground-state to ground-state β-decay would have been reduced significantly. As with the thought on the potential re-measurement of decays of ^{113}Ba in the future, a new configuration of detectors is under development aimed at observation of ground-state β-decays of ^{113}Ba. In the new design, a segmented inorganic scintillator (e.g. YAP or YSO) crystal coupled to a position-sensitive photo multiplier (PSPMT) will be placed closely behind the DSSD to enable position correlation between ion implantation and subsequent β-decay. This will improve the sensitivity of the setup for $^{113}\text{Ba} \rightarrow {}^{113}\text{Cs}$ decay channel and enable its unambiguous identification.

Bibliography

[1] LU Xiting. *Nuclear physics*. Beijing: Atomic Energy Press, 2000. 2

[2] Hans Geiger and JM Nuttall. Lvii. the ranges of the α particles from various radioactive substances and a relation between range and period of transformation. *The London, Edinburgh, and Dublin Philosophical Magazine and Journal of Science*, 22(130):613–621, 1911. 3

[3] G. Gamow. Zur quantentheorie der atomzertrümmerung. *Zeitschrift für Physik*, 52(7):510–515, Jul 1929. 3

[4] Maria Goeppert Mayer. On closed shells in nuclei. ii. *Physical Review*, 75(12):1969, 1949. 4

[5] Roger D Woods and David S Saxon. Diffuse surface optical model for nucleon-nuclei scattering. *Physical Review*, 95(2):577, 1954. 4

[6] Luc Valentin. Subatomic physics: nuclei and particles. 1981. 4

[7] R.G. Lovas, R.J. Liotta, A. Insolia, K. Varga, and D.S. Delion. Microscopic theory of cluster radioactivity. *Physics Reports*, 294(5):265 – 362, 1998. 6

[8] John O Rasmussen. Alpha-decay barrier penetrabilities with an exponential nuclear potential: even-even nuclei. *Physical Review*, 113(6):1593, 1959. 6

[9] Z. Janas, C. Mazzocchi, L. Batist, A. Blazhev, M. Górska, M. Kavatsyuk, O. Kavatsyuk, R. Kirchner, A. Korgul, M. La Commara, K. Miernik, I. Mukha, A. Płochocki, E. Roeckl, and K. Schmidt. Measurements of 110xe and 106te decay half-lives. *The European Physical Journal A - Hadrons and Nuclei*, 23(2):197–200, Feb 2005. 6

[10] HJ Mang. Alpha decay. *Annual Review of Nuclear Science*, 14(1):1–26, 1964. 7

[11] Chang Xu, G Röpke, P Schuck, Zhongzhou Ren, Y Funaki, H Horiuchi, A Tohsaki, T Yamada, and Bo Zhou. α-cluster formation and decay in the quartetting wave function approach. *Physical Review C*, 95(6):061306, 2017. 7

[12] Chong Qi. Alpha decay as a probe for the structure of neutron-deficient nuclei. *Reviews in Physics*, 1:77 – 89, 2016. 8

[13] C. Qi, A. N. Andreyev, M. Huyse, R. J. Liotta, P. Van Duppen, and R. A. Wyss. Abrupt changes in α-decay systematics as a manifestation of collective nuclear modes. *Phys. Rev. C*, 81:064319, Jun 2010. 8

[14] Chart of nuclides. `http://www.nndc.bnl.gov/chart/`. 8

[15] Ronald D Macfarlane and Antti Siivola. New region of alpha radioactivity. *Physical Review Letters*, 14(4):114, 1965. 8

[16] E Roeckl. Alpha radioactivity. *Radiochimica Acta*, 70(s1):107–122, 1995. 8

[17] D.S. Delion, A. Insolia, and R.J. Liotta. Photon-neutron correlations and microscopic description of alpha decay. *Nuclear Physics A*, 549(3):407 – 419, 1992. 9

[18] Z.X. Xu, C. Qi, J. Blomqvist, R.J. Liotta, and R. Wyss. Multistep shell model description of spin-aligned neutronproton pair coupling. *Nuclear Physics A*, 877:51 – 58, 2012. 9

[19] R Id Betan and Witold Nazarewicz. α decay in the complex-energy shell model. *Physical Review C*, 86(3):034338, 2012. 9, 11

[20] S. N. Liddick, R. Grzywacz, C. Mazzocchi, R. D. Page, K. P. Rykaczewski, J. C. Batchelder, C. R. Bingham, I. G. Darby, G. Drafta, C. Goodin, C. J. Gross, J. H. Hamilton, A. A. Hecht, J. K. Hwang, S. Ilyushkin, D. T. Joss, A. Korgul, W. Królas, K. Lagergren, K. Li, M. N. Tantawy, J. Thomson, and J. A. Winger. Discovery of ^{109}Xe and ^{105}Te: Superallowed α decay near doubly magic ^{100}Sn. *Phys. Rev. Lett.*, 97:082501, Aug 2006. 10, 11, 24

[21] I. G. Darby, R. K. Grzywacz, J. C. Batchelder, C. R. Bingham, L. Cartegni, C. J. Gross, M. Hjorth-Jensen, D. T. Joss, S. N. Liddick, W. Nazarewicz, S. Padgett, R. D. Page, T. Papenbrock, M. M. Rajabali, J. Rotureau, and K. P. Rykaczewski. Orbital

dependent nucleonic pairing in the lightest known isotopes of tin. *Phys. Rev. Lett.*, 105:162502, Oct 2010. 10, 24, 43, 67

[22] L. Capponi, J. F. Smith, P. Ruotsalainen, C. Scholey, P. Rahkila, K. Auranen, L. Bianco, A. J. Boston, H. C. Boston, D. M. Cullen, X. Derkx, M. C. Drummond, T. Grahn, P. T. Greenlees, L. Grocutt, B. Hadinia, U. Jakobsson, D. T. Joss, R. Julin, S. Juutinen, M. Labiche, M. Leino, K. G. Leach, C. McPeake, K. F. Mulholland, P. Nieminen, D. O'Donnell, E. S. Paul, P. Peura, M. Sandzelius, J. Sarén, B. Saygi, J. Sorri, S. Stolze, A. Thornthwaite, M. J. Taylor, and J. Uusitalo. Direct observation of the ^{114}Ba $\rightarrow^{110}$ Xe $\rightarrow^{106}$ Te $\rightarrow^{102}$ Sn triple α-decay chain using position and time correlations. *Phys. Rev. C*, 94:024314, Aug 2016. 10, 11

[23] F Heine, T Faestermann, A Gillitzer, and HJ Körner. Proceedings of the 6th international conference on nuclei far from stability and 9th international conference on atomic masses and fundamental constants, bernkastel-kues, germany, 1992. 1992. 10

[24] WN Lennard, H Geissel, KB Winterbon, D Phillips, TK Alexander, and JS Forster. Nonlinear response of si detectors for low-z ions. *Nuclear Instruments and Methods in Physics Research Section A: Accelerators, Spectrometers, Detectors and Associated Equipment*, 248(2-3):454–460, 1986. 10

[25] R. D. Page, P. J. Woods, R. A. Cunningham, T. Davinson, N. J. Davis, A. N. James, K. Livingston, P. J. Sellin, and A. C. Shotter. Alpha radioactivity above ^{100}Sn including the decay of ^{108}I. *Phys. Rev. C*, 49:3312–3315, Jun 1994. 10

[26] D Schardt, T Batsch, R Kirchner, O Klepper, W Kurcewicz, E Roeckl, and P Tidemand-Petersson. Alpha decay of neutron-deficient isotopes with 52 z 55, including the new isotopes 106te (t12= 60 μs) and 110xe. *Nuclear Physics A*, 368(1):153–163, 1981. 10

[27] Georges Audi, AH Wapstra, and C Thibault. The ame2003 atomic mass evaluation:(ii). tables, graphs and references. *Nuclear physics A*, 729(1):337–676, 2003. 10

[28] E Roeckl, GM Gowdy, R Kirchner, O Klepper, A Piotrowski, A Płochocki, W Reisdorf, P Tidemand-Petersson, J Żylicz, D Schardt, et al. The decay of 0.57 s 114 cs. *Zeitschrift für Physik A Hadrons and Nuclei*, 294(3):221–232, 1980. 10

[29] C. Mazzocchi, R. Grzywacz, S. N. Liddick, K. P. Rykaczewski, H. Schatz, J. C. Batchelder, C. R. Bingham, C. J. Gross, J. H. Hamilton, J. K. Hwang, S. Ilyushkin, A. Korgul, W. Królas, K. Li, R. D. Page, D. Simpson, and J. A. Winger. α. *Phys. Rev. Lett.*, 98:212501, May 2007. 10

[30] E. Roeckl, R. Kirchner, O. Klepper, G. Nyman, W. Reisdorf, D. Schardt, K. Wien, R. Fass, and S. Mattsson. A new island of -emission: -decay energies and widths of neutron deficient tellurium, iodine and xenon isotopes. *Physics Letters B*, 78(4):393 – 396, 1978. 10

[31] R Kirchner, O Klepper, G Nyman, W Reisdorf, E Roeckl, D Schardt, N Kaffrell, P Peuser, and K Schneeweiss. New neutron-deficient tellurium, iodine, and xenon isotopes produced by reactions of 290 mev 58ni ions on 58ni and 63cu targets. *Physics Letters B*, 70(2):150–154, 1977. 10

[32] Ch Mazzocchi, Z Janas, L Batist, V Belleguic, J Döring, M Gierlik, M Kapica, R Kirchner, GA Lalazissis, H Mahmud, et al. Alpha decay of 114 ba. *Physics Letters B*, 532(1):29–36, 2002. 10, 11, 64

[33] Chang Xu and Zhongzhou Ren. Half lives of α-emitters approaching the n= z line. *Physical Review C*, 74(3):037302, 2006. 11, 12, 64

[34] AA Hecht, CJ Lister, CN Davids, A Heinz, N Hoteling, C Mazzocchi, J Palombo, D Seweryniak, J Shergur, M Stoyer, et al. Search for enhanced alpha preformation in the n= z+ 1 nuclei 113ba, 109xe, 105te. In *AIP Conference Proceedings*, volume 819, pages 355–359. AIP, 2006. 11

[35] Z Janas, A Płochocki, J Szerypo, R Collatz, Z Hu, H Keller, R Kirchner, O Klepper, E Roeckl, K Schmidt, et al. Decay studies of the neutron-deficient isotopes 114–118ba. *Nuclear Physics A*, 627(1):119–136, 1997. 11

[36] A Guglielmetti, R Bonetti, G Poli, PB Price, AJ Westphal, Z Janas, H Keller, R Kirchner, O Klepper, A Piechaczek, et al. Identification of the new isotope ba 114 and search for its α and cluster radioactivity. *Physical Review C*, 52(2):740, 1995. 11

[37] A Korgul, Krzysztof Piotr Rykaczewski, Carl J Gross, RK Grzywacz, SN Liddick, C Mazzocchi, JC Batchelder, CR Bingham, IG Darby, C Goodin, et al. Toward sn 100: Studies of excitation functions for the reaction between ni 58 and fe 54 ions. *Physical Review C*, 77(3):034301, 2008. 12

[38] P Möller, JR Nix, and KL Kratz. Atomic data nucl. *Data Tables*, 66(131):749, 1997. 12, 65

[39] Jaea tandem accelerator. `https://www.jaea.go.jp/english/04/ntokai/kasokuki/kasokuki_04.html`. 14

[40] S Mitsuoka, H Ikezoe, K Nishio, K Satou, and L Dan. The present and the future of jaeri recoil mass separator. *Journal of Nuclear and Radiochemical Sciences*, 3(1):209–211, 2002. 16

[41] Digital gamma finder(dgf) pixie-16. `http://www.xia.com/Manuals/Pixie16UserManual.pdf`. 22, 48

[42] R. Grzywacz, C.J. Gross, A. Korgul, S.N. Liddick, C. Mazzocchi, R.D. Page, and K. Rykaczewski. Rare isotope discoveries with digital electronics. *Nuclear Instruments and Methods in Physics Research Section B: Beam Interactions with Materials and Atoms*, 261(1):1103 – 1106, 2007. The Application of Accelerators in Research and Industry. 23

[43] K-H Schmidt, C-C Sahm, K Pielenz, and H-G Clerc. Some remarks on the error analysis in the case of poor statistics. *Zeitschrift für Physik A Hadrons and Nuclei*, 316(1):19–26, 1984. 26, 55

[44] Karl-Heinz Schmidt. A new test for random events of an exponential distribution. *The European Physical Journal A-Hadrons and Nuclei*, 8(1):141–145, 2000. 27

[45] James F Ziegler, MD Ziegler, and JP Biersack. Srim–the stopping and range of ions in matter (2010). *Nuclear Instruments and Methods in Physics Research Section B: Beam Interactions with Materials and Atoms*, 268(11):1818–1823, 2010. 29

[46] MJ Berger, SM Seltzer, SE Chappell, JC Humphreys, and JW Motz. Response of silicon detectors to monoenergetic electrons with energies between 0.15 and 5.0 mev. *Nuclear Instruments and Methods*, 69(2):181–193, 1969. 38

[47] Martin J Berger. Estar, pstar, and astar: Computer programs for calculating stopping-power and range tables for electrons, protons, and helium ions. *Unknown*, 1992. 38

[48] W Reisdorf. Analysis of fissionability data at high excitation energies. *Zeitschrift für Physik A Atoms and Nuclei*, 300(2-3):227–238, 1981. 44

[49] W Reisdorf and M Schädel. How well do we understand the synthesis of heavy elements by heavy-ion induced fusion? *Zeitschrift für Physik A Hadrons and Nuclei*, 343(1):47–57, 1992. 44

[50] H Tan, M Momayezi, A Fallu-Labruyere, YX Chu, and WK Warburton. A fast digital filter algorithm for gamma-ray spectroscopy with double-exponential decaying scintillators. *IEEE Transactions on Nuclear Science*, 51(4):1541–1545, 2004. 61

[51] Hiroyuki Koura. Phenomenological formula for alpha-decay half-lives. *Journal of nuclear science and technology*, 49(8):816–823, 2012. 63

[52] C. Qi, F. R. Xu, R. J. Liotta, and R. Wyss. Universal decay law in charged-particle emission and exotic cluster radioactivity. *Phys. Rev. Lett.*, 103:072501, Aug 2009. 64

[53] BA Brown and WDM Rae. The shell-model code nushellx@ msu. *Nuclear Data Sheets*, 120:115–118, 2014. 67

[54] P. Hornshj, K. Wilsky, P.G. Hansen, B. Jonson, and O.B. Nielsen. Beta-delayed proton emission from heavy nuclei: (ii). the calculation of spectral shapes and intensities in a compound-nucleus model. *Nuclear Physics A*, 187(3):609 – 623, 1972. 69

Vita

Yongchi Xiao was born in Fuzhou, China in 1990. He spent his childhood in this warm and lovely city in southern China. At the age of 15, he went to the legendary Fuzhou No.1 high school where he made up his mind to be a diplomat. At the age of 18, he entered Nankai University in Tianjin, China and surprisingly became a student in physics, which had not been anticipated ever before. Great interest with passion was found in physics shortly afterwards. Majoring in optics and photonics for years, he switched to work on plasma physics as his bachelor's thesis program. At the age of 22, he came to the University of Tennessee and joined the low energy nuclear structure group under the direction of Dr. Robert Grzywacz. His effort was concentrated on α-decays in ^{100}Sn region and was associated with experimental activities in ORNL and JAEA. In December 2017, he completed the requirements for doctoral degree in physics.